JGR Atmospheres

RESEARCH ARTICLE
10.1029/2020JD034180

Special Section:
Fire in the Earth System

Evaluation of Novel NASA Moderate Resolution Imaging Spectroradiometer and Visible Infrared Imaging Radiometer Suite Aerosol Products and Assessment of Smoke Height Boundary Layer Ratio During Extreme Smoke Events in the Western USA

S. Marcela Loría-Salazar[1,2], Andrew M. Sayer[3,4], John Barnes[5], Jingting Huang[2,6], Connor Flynn[1], Neil Lareau[2], Jaehwa Lee[3,7], Alexei Lyapustin[3], Jens Redemann[1], Ellsworth J. Welton[3], Joseph L. Wilkins[8,9], and Heather A. Holmes[2,6]

[1]School of Meteorology, University of Oklahoma, Norman, OK, USA, [2]Atmospheric Sciences Program, Department of Physics, University of Nevada, Reno, Reno, NV, USA, [3]NASA Goddard Space Flight Center, Greenbelt, MD, USA, [4]Goddard Earth Science Technology and Research, Universities Space Research Association, Columbia, MD, USA, [5]NOAA Global Monitoring Laboratory, Boulder, CO, USA, [6]Department of Chemical Engineering, University of Utah, Salt Lake City, UT, USA, [7]Earth System Science Interdisciplinary Center, University of Maryland, College Park, MD, USA, [8]U.S. Environmental Protection Agency, Durham, NC, USA, [9]Pacific Wildland Fire Sciences Laboratory, School of Environmental and Forest Sciences, University of Washington, Seattle, WA, USA

Abstract We analyze new aerosol products from NASA satellite retrievals over the western USA during August 2013, with special attention to locally generated wildfire smoke and downwind plume structures. Aerosol optical depth (AOD) at 550 nm from MODerate Resolution Imaging Spectroradiometer (MODIS) (Terra and Aqua Collections 6 and 6.1) and Visible Infrared Imaging Radiometer Suite (VIIRS) Deep Blue (DB) and MODIS (Terra and Aqua) Multi-Angle Implementation of Atmospheric Correction (MAIAC) retrievals are evaluated against ground-based AErosol RObotic NETwork (AERONET) observations. We find a significant improvement in correlation with AERONET and other metrics in the latest DB AOD (MODIS C6.1 $r^2 = 0.75$, VIIRS $r^2 = 0.79$) compared to MODIS C6 ($r^2 = 0.62$). In general, MAIAC ($r^2 = 0.84$) and DB (MODIS C6.1 and VIIRS) present similar statistical evaluation metrics for the western USA and are useful tools to characterize aerosol loading associated with wildfire smoke. We also evaluate three novel NASA MODIS plume injection height (PIH) products, one from MAIAC and two from the Aerosol Single scattering albedo and layer Height Estimation (ASHE) (MODIS and VIIRS) algorithm. Both Terra and Aqua MAIAC PIHs statistically agree with ground-based and satellite lidar observations near the fire source, as do ASHE, although the latter is sensitive to assumptions about aerosol absorption properties. We introduce a first-order approximation Smoke Height Boundary Layer Ratio (SHBLR) to qualitatively distinguish between aerosol pollution within the planetary boundary layer and the free troposphere. We summarize the scope, limitations, and suggestions for scientific applications of surface level aerosol concentrations specific to wildfire emissions and smoke plumes using these novel NASA MODIS and VIIRS aerosol products.

Key Points:

- Aerosol optical depth and plume injection height products from new collections of Moderate resolution imaging spectroradiometer and Visible Infrared Imaging Radiometer Suite demonstrate improved capabilities for smoke events
- New Smoke Height Boundary Layer Ratio indicates when wildfire smoke aerosols are likely to be confined within the planetary boundary layer
- Heterogeneous vertical aerosol profiles were found downwind of wildfires induced by mountainous terrain and complex boundary layer physics

Supporting Information:

Supporting Information may be found in the online version of this article.

Correspondence to:

S. M. Loría-Salazar,
mloria@ou.edu

Citation:

Loría-Salazar, S. M., Sayer, A. M., Barnes, J., Huang, J., Flynn, C., Lareau, N., et al. (2021). Evaluation of novel NASA MODerate Resolution Imaging Spectroradiometer and Visible Infrared Imaging Radiometer Suite aerosol products and assessment of smoke height boundary layer ratio during extreme smoke events in the western USA. *Journal of Geophysical Research: Atmospheres*, *126*, e2020JD034180. https://doi.org/10.1029/2020JD034180

Received 22 NOV 2020
Accepted 22 APR 2021

Author Contributions:

Conceptualization: S. Marcela Loría-Salazar, Andrew M. Sayer, Alexei Lyapustin, Heather A. Holmes
Data curation: S. Marcela Loría-Salazar, John Barnes, Jingting Huang, Alexei Lyapustin, Ellsworth J. Welton

1. Introduction

Air quality (AQ) awareness has increased in the past several decades because of the growing body of literature citing adverse impacts of aerosol pollution on human health (Alman et al., 2016; Lim et al., 2012) and the impacts of aerosols on climate change by altering Earth's radiative budget (Stocker et al., 2013). Ground-based monitoring networks have been established with the aim of measuring surface (Pitchford et al., 2007) and column-integrated loadings of particulate matter (PM) and aerosols, respectively (Snider et al., 2015). Monitoring stations are considered "ground-truth," but they are a single point of observation and offer limited information about meso and synoptic scales of aerosol pollution (Gupta et al., 2006; Hoff & Christopher, 2009).

Satellite characterization of aerosol pollution improves the spatial and temporal sampling as many locations have few or no existing stations (Hoff & Christopher, 2009; Streets et al., 2013). Models have been developed

Formal analysis: S. Marcela Loría-Salazar, Andrew M. Sayer, Jaehwa Lee, Heather A. Holmes
Funding acquisition: S. Marcela Loría-Salazar, Jens Redemann
Investigation: S. Marcela Loría-Salazar, Jaehwa Lee, Alexei Lyapustin, Heather A. Holmes
Methodology: S. Marcela Loría-Salazar, Alexei Lyapustin, Heather A. Holmes
Project Administration: S. Marcela Loría-Salazar, Jens Redemann, Heather A. Holmes
Resources: S. Marcela Loría-Salazar, Andrew M. Sayer, John Barnes, Connor Flynn, Neil Lareau, Alexei Lyapustin, Ellsworth J. Welton, Heather A. Holmes
Software: S. Marcela Loría-Salazar, Heather A. Holmes
Supervision: S. Marcela Loría-Salazar, Andrew M. Sayer, Heather A. Holmes
Validation: S. Marcela Loría-Salazar, John Barnes, Ellsworth J. Welton, Heather A. Holmes
Visualization: S. Marcela Loría-Salazar, Jingting Huang, Connor Flynn, Jaehwa Lee, Alexei Lyapustin
Writing – original draft: S. Marcela Loría-Salazar, Andrew M. Sayer, Jaehwa Lee, Alexei Lyapustin, Heather A. Holmes
Writing – review & editing: S. Marcela Loría-Salazar, Andrew M. Sayer, Connor Flynn, Jaehwa Lee, Jens Redemann, Joseph L. Wilkins, Heather A. Holmes

to relate observations of columnar aerosol optical depth (AOD) and surface $PM_{2.5}$ (PM with an aerodynamic diameter smaller than 2.5 μm) based on empirical relationships (Gupta et al., 2006; Hu et al., 2014; Murray et al., 2019; Nabavi et al., 2019; Wang & Christopher, 2003). These empirical models, based on linear and non-linear regressions, have shown lower uncertainties in predicted $PM_{2.5}$ in the eastern USA compared to other locations due to the strong association between AOD and $PM_{2.5}$ in this region (e.g., Li et al., 2015). However, in the western USA, these models are challenged by complex atmospheric physics and air pollution characteristics (Li et al., 2015; Loría-Salazar et al., 2017; Pierce et al., 2019).

Aerosol pollution in the western USA is characterized by wildfires, anthropogenic emissions, and biogenic emissions (Griffin et al., 1999; Hoffmann et al., 1997) that mix with urban air and transboundary pollution from Eurasia (Parrish et al., 2010; Pierce et al., 2018). Severe droughts in recent years (2006–2017 and again in 2020–2021) have driven an increasing number of wildfires (Crockett & Westerling, 2017; Kogan & Guo, 2015), especially in California (Blunden & Arndt, 2020; Stephens & Collins, 2004; Stephens & Fry, 2005; US Drought Monitor, 2020; Westerling, 2016; Westerling et al., 2006). Because of high temperatures, earlier snowmelt, less rainfall, and drought conditions, thousands of acres in the western USA have been affected by multiple fires generating vast amounts of aerosol pollution (Bian et al., 2020; Brewer & Clements, 2020; Scasta et al., 2016). The smoke plumes produced by those fires undergo complex aerosol transport processes typical of the western US, leading to a potential disconnect between aerosol measurements at the surface (i.e., $PM_{2.5}$ concentrations) and the aerosol concentrations aloft (Wilkins et al., 2020). Smoke plume injection, boundary layer mixing, and entrainment aloft can disperse the smoke plumes into the free troposphere.

Wildfires are important to maintain the ecological equilibrium of the landscape in the western USA. However, smoke exposure is a growing global public health problem, which especially affects vulnerable populations (Cascio, 2017). In general, satellite-based AQ studies are challenged during fire periods for a number of reasons: (a) the difficulties of satellite algorithms in detecting small fires diminishes the accuracy of satellite-derived AQ studies (Hao & Larkin, 2014); (b) large fire events can produce pyrocumulus clouds, which in turn can prevent AOD retrievals (Peterson et al., 2014, 2017); (c) high surface reflectance, which can increase AOD retrieval uncertainty; (d) a wide variety in smoke optical properties, leading to regional biases in retrievals (Eck et al., 2013; Sayer et al., 2014); and (e) satellite retrieval pixel selection criteria, which can lead to unintended exclusion of high-AOD, heterogeneous aerosol plumes (Loría-Salazar et al., 2016; Lyapustin et al., 2018; Shi et al., 2019). In addition, using satellite-derived aerosol products has led to an underestimation of aerosol concentrations during fire cases (Saide et al., 2015). Unresolved uncertainties in modeling the AQ associated with wildfires (e.g., statistical data-fusion, chemical transport modeling) include capturing how wind patterns transport the smoke from a wildfire to other areas and quantifying its potential health impacts (e.g., Wilkins et al., 2020). Specific to chemical transport models (CTM), these challenges are related, in part, to the high uncertainties in both the smoke plume injection height and vertical distribution of smoke (i.e., aerosols or PM) concentration used to estimate the wildfire emissions (Liu et al., 2018, 2019; Paugam et al., 2016; Wilkins et al., 2018).

New versions of aerosol products from the MODerate Resolution Imaging Spectroradiometer (MODIS) and Visible Infrared Imaging Radiometer Suite (VIIRS) instruments showed a better characterization of wildfire smoke from remote sensing platforms with respect to previous collections (Hsu et al., 2019; Sayer et al., 2019). This study analyzes the new NASA MODIS and VIIRS Deep Blue (DB) and MODIS Collection 6 (C6) Multi-Angle Implementation of Atmospheric Correction (MAIAC) aerosol products, fire radiative power (FRP), and Aerosol Single scattering albedo and layer Height Estimation (ASHE) satellite algorithms over extreme wildfire smoke events in August 2013. The main goal is to evaluate NASA MODIS and VIIRS aerosol loading and PIH products using ground-based sun photometry and lidar data. In addition, a comparison between MODIS and VIIRS fire intensity products is included to understand the differences between the retrievals of the two satellite instruments.

Multiple data sources from both routine monitoring networks and satellite aerosol products, discussed in Section 2. Section 3 presents a new metric to assess the aerosol pollution at the surface versus aloft downwind from sources such as wildfires. Section 4 analyzes the spatial-temporal distribution of the satellite retrievals. Section 5 presents an evaluation of satellite smoke plume injection height retrievals and their relevance for AQ modeling. Sections 6 and 7 gives a summary of the findings.

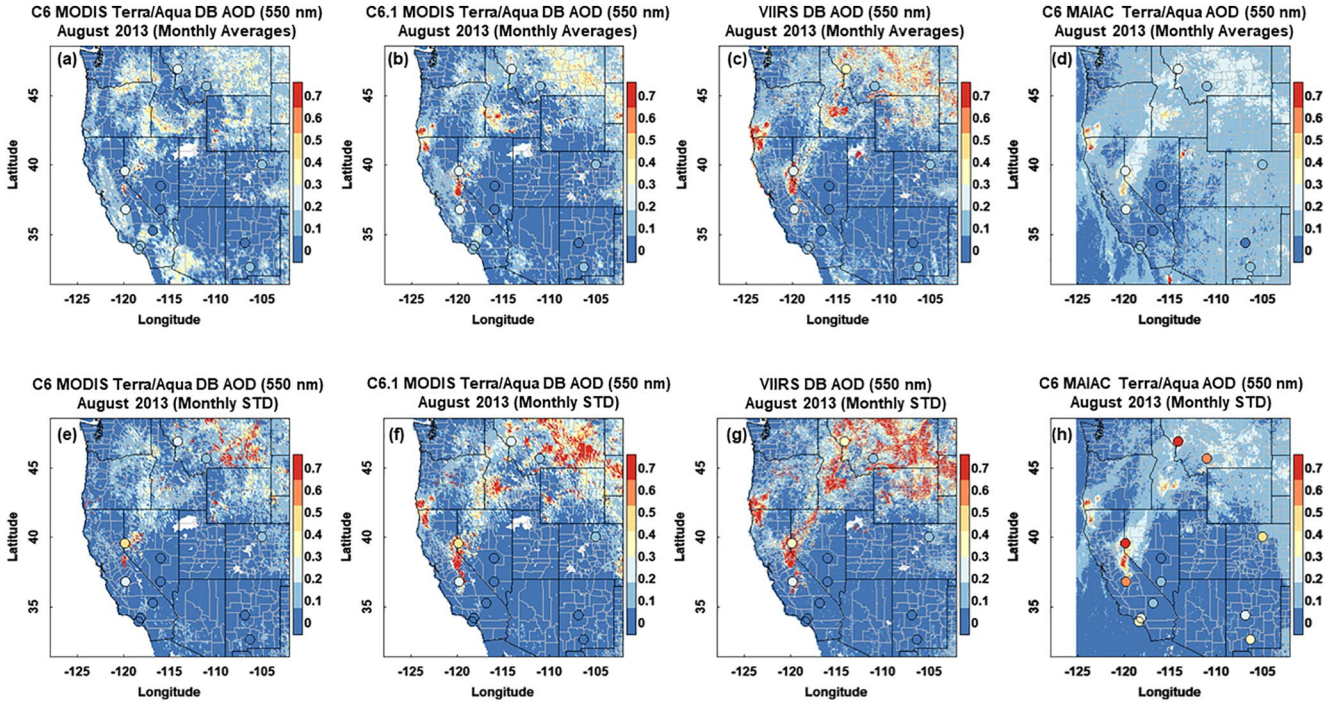

Figure 1. Monthly averages and standard deviations (STD) of satellite AOD products (mapped data) and AERONET (circles) during August 2013. The AERONET stations selected had at least 70% temporal coverage. (a–d) Monthly averages of algorithms for Deep Blue (DB) MODIS C6, DB Col. MODIS 6.1, DB VIIRS, and MODIS MAIAC. (e–h) Monthly standard deviations of algorithms for DB MODIS C6, DB Col. MODIS 6.1, DB VIIRS, and MODIS MAIAC. AOD, aerosol optical depth; MAIAC, multi-angle implementation of atmospheric correction; MODIS, MODerate Resolution Imaging Spectroradiometer; VIIRS, Visible Infrared Imaging Radiometer Suite.

2. Instruments, Datasets, and Atmospheric Models

This research used ground-based measurements (aerosol parameters and weather variables), satellite aerosol retrievals, and model outputs to investigate and evaluate the horizontal and vertical extent of smoke from wildfires in the western USA during August 2013.

2.1. Ground-Based AQ Measurements

Ground-based AOD measurements from the NASA AERONET Network were used to evaluate the satellite AOD (Holben et al., 1998, 2001). The Cimel CE-318 is the standard instrument used in AERONET to retrieve AOD. Direct solar irradiance at 440, 500, and 675 nm were measured using the Cimel CE-318 sun photometer at 13 AERONET sites in California, Nevada, Montana, Colorado, and New Mexico (Figure 1, circles; for locations and elevations of each station, see Table SI.1). Original spectral AOD datasets from AERONET (version 3) were interpolated to 550 nm (Eck et al., 1999). AERONET AOD absolute uncertainty in the mid-visible is ~0.01 (Eck et al., 1999). See Giles et al. (2019) for improvements in this recently released version 3 of the AERONET record.

Ground-based lidar measurements were used to evaluate satellite-derived plume injection height (PIH). Total attenuated backscattering was measured using a ground-based Doppler lidar (Halo Photonics, Ltd., Streamline 75) from the California State University Mobile Atmospheric Profiling System (CSU-MAPS; Clements & Oliphant, 2014). In addition, lidar signal data from a Micro Pulse Lidar (527 nm with no polarization; Campbell et al., 2002) at the Trinidad Head site was collected as part of the NASA Micro-Pulse Lidar Network (MPLNET; Welton et al., 2001). MPLNET is an international network designed to measure aerosol and cloud vertical structures and boundary layer depth.

Surface $PM_{2.5}$ mass concentrations were collected using an automatic Beta Attenuation Monitor (BAM) from the regulatory monitoring networks maintained by the local AQ management agencies. The data were

accessed from the US Environmental Protection Agency (EPA) AQ System (AQS) for Fresno, CA (36.79°N, −119.77°W), Trinidad Head, CA (41.05°N, −124.15°W), and Reno, NV (39.53°N, −119.81°W). The BAM measures $PM_{2.5}$ mass concentrations through a size-selective inlet, a filter tape, a beta radiation source, and a beta radiation detector (Chung et al., 2001). The lower detection limit for $PM_{2.5}$ concentrations using the BAM instrument is 2 $\mu g\ m^{-3}$.

2.2. Planetary Boundary Layer Height

Planetary boundary layer height (PBLH) was modeled using the Weather Research and Forecasting (WRF) model, a mesoscale numerical weather prediction model. For our use, the WRF model had an outer domain extending over the continental USA with 12-km horizontal resolution, nudged with observations from weather stations as well as balloon soundings (Michalakes et al., 1998, 2004). Where available, the vertical potential temperature profiles from balloon soundings were also used to determine the PBLH. The vertical potential temperature gradient method was used to determine the height of the temperature inversion layer (capping layer) above a deep, well-mixed planetary boundary layer, as is often observed in the late afternoon during warm periods, such as summer (Stull, 1988). Details of the boundary conditions (NAM 12-km resolution), land-surface data set (USGS), and the WRF model configuration are in Loría-Salazar et al., (2017). The results of the WRF model evaluation are in Figures SI.4–SI.23. Locations and elevations of each balloon sounding station and further comparisons of PBLH from WRF outputs and balloon soundings are in Table SI.1.

2.3. AOD From Satellite Retrievals

We used AOD retrievals at 550 nm from both MODIS sensors (on board the Terra and Aqua satellites) and the VIIRS sensor on the Suomi National Polar-orbiting Partnership (SNPP) satellite. Terra has a 10:30 daytime local solar Equatorial crossing time; Aqua and SNPP have 1:30 p.m. local solar Equatorial crossing times, but are on different orbital cycles.

Several NASA aerosol products are available from these sensors. First, we used the recently released MODIS Terra and Aqua Collection 6.1 (C6.1) and SNPP VIIRS version 1 Deep Blue (DB) (Hsu et al., 2019) data sets. We also used the previous MODIS Collection 6 (C6) DB, to examine the effect of algorithm updates between the two versions on the AOD. Validation of these DB datasets was performed in Sayer et al. (2013, 2019) and, as recommended there, we only used retrievals with the highest quality flags (2 and 3). Second, we used the current MODIS Terra and Aqua C6 MAIAC data set (Lyapustin et al., 2012, 2018). The AOD is provided at nominal $10 \times 10\ km^2$ horizontal pixel size at nadir from MODIS DB, $6 \times 6\ km^2$ from VIIRS DB (with pixel sizes increasing for off-nadir views), and on a $1 \times 1\ km^2$ uniform grid from MAIAC. The NASA Dark Target algorithm was not used in this investigation because of its known performance limitations at retrieving AOD over bright surfaces, which are common in the western USA (Loría-Salazar et al., 2016).

The DB algorithm performs aerosol retrievals on individual MODIS and VIIRS pixels. Surface reflectance is assumed from climatological database over stable (typically arid) locations, and from a dynamic spectral surface reflectance model over other (typically vegetated) surfaces (Hsu et al., 2019). In contrast, MAIAC composites MODIS Terra and Aqua data in time and, under the assumption that surface reflectance is fairly temporally stable, simultaneously retrieves atmospheric aerosol and surface reflectance properties for the composited data. Both algorithms make regional and seasonal assumptions about some aerosol properties (e.g., size and absorption).

For simplicity, uncertainties for these AOD retrievals are often expressed as an "expected error" (EE). The goal is that the EE encompasses ±1 standard deviation (about 68%) of matchups with AERONET (Giles et al., 2019; Sayer, 2020). For DB AOD at 550 nm this goal EE is ±(0.05 + 0.2xAOD); for C6 DB about 80% of retrievals in the western USA fell into this envelope (Hsu et al., 2013; Sayer et al., 2013), while for C6.1 and VIIRS 83%–84% do (Sayer et al., 2019). This implies that the true EE in this region is somewhat lower than the global goal. For MAIAC, Lyapustin et al., (2018) concluded that the EE for AOD at 550 nm in the western USA region is ±(0.034 + 0.13xAOD).

2.4. Aerosol Back Scatter Products From Satellite Retrievals

Cloud-Aerosol Lidar with Orthogonal Polarization (CALIOP)-attenuated backscatter profile data were collected from the Cloud-Aerosol Lidar and Infrared Pathfinder Satellite Observation (CALIPSO) satellite, Version 4, to study vertical aerosol distribution. Profile data consist of total attenuated backscatter coefficient at 532 nm and depolarization ratio from the CALIOP 5-km aerosol profile product (Kim et al., 2018). To extract the backscatter signal associated with aerosol features from these profiles, we screened out all features that either were not aerosols (feature type and subtype equal to 3) or that had low confidence that the feature was an aerosol (cloud-aerosol discrimination score >-20).

2.5. Satellite-Derived Plume Injection Height (PIH)

Three PIH datasets were used in this study (a) MAIAC, (b) MODIS ASHE, and (c) VIIRS ASHE. ASHE uses satellite inputs from MODIS or VIIRS (AOD and Ångström exponent, AE) in combination with Ozone Monitoring Instrument (OMI) or Ozone Mapping and Profiling Suite (OMPS) UV aerosol index (UVAI), as well as (optionally) CALIOP aerosol layer height (Lee et al. 2015, 2016). Here, references to MODIS ASHE indicate the combination of MODIS AOD/AE and OMI UVAI, while references to VIIRS ASHE indicate VIIRS DB AOD/AE and OMPS UVAI. ASHE can provide aerosol height over broad areas, including both near-source and transported plumes, complementary to existing datasets. The algorithm can be applied to absorbing aerosols, including smoke, dust storms, and volcanic ash (Jeong & Hsu 2008; Lee et al., 2015). Aerosol single scattering albedo (SSA) must be assumed, unless CALIOP data are used as input, in which case a scene-average SSA is retrieved in addition to aerosol height. The EE envelope for plume height is expected to be ± 1 km for well-characterized (in terms of aerosol loading and SSA), optically thick plumes (Lee et al., 2016).

The C6 MAIAC algorithm uses thermal contrasts (at 11 μm) between the smoke plume and smoke-free background, then assumes an average lapse rate (6.5 C km^{-1}) to evaluate an effective plume height. The thermal contrast is created by the absorption of gases emitted during the combustion phase and their entrainment into the rising plume. This method is used because fine-mode smoke aerosol is transparent at 11 μm. A PIH is computed when smoke is "thick enough"; that is, AOD ≥0.8 at 470 nm. The MAIAC thermal technique has been validated against both stereoscopic Multi-angle Imaging SpectroRadiometer (MISR) MINX and CALIOP lidar data (within about 500 m) near plume sources such as active fires; however, the method is unreliable for smoke transported further away from sources (Lyapustin et al., 2020).

2.6. MODIS Fire Radiative Power

The NASA MODIS and VIIRS fire detection FRP product (Giglio et al., 2016) was used to estimate biomass burning frequency and power during the month of August 2013 at the satellite overpass times. The detection algorithm identifies pixels which contain one or more active fires using the brightness temperature (BT) at three spectral channels for daytime (nighttime) at 0.65, 0.86, and 2.1 μm (4, 11, and 12 μm) at 1 km resolution. FRP is then estimated from the 4 μm BT (Giglio et al., 2016). FRP is included in this investigation because multiple emission inventories use FRP to parameterize biomass burning (i.e., wildfires, prescribed burning, and agricultural burning) intensity, and emissions (e.g., Fisher et al., 2020; Kaiser et al., 2012).

2.7. MODIS Albedo Retrievals

The effect of surface reflectance on the satellite AOD retrievals was investigated using white-sky (Lambertian) surface albedo at 650 nm from the operational MODIS Bidirectional Reflectance Distribution Function (BRDF) and albedo products (Schaaf et al., 2002). These combine MODIS Terra and Aqua observations provide BRDF parameters and albedo every 16 days at 1 km resolution. Previous investigations showed that surface reflectance hotspots not captured in AOD retrieval algorithm surface parameterizations can lead to unrealistically high AOD retrievals (Boehmler et al., 2018; Huang et al., 2021; Loría-Salazar et al., 2016). These unrealistically high AODs can be misinterpreted as extreme aerosol events such as smoke from wildfires. For this reason, this investigation qualitatively compares AOD hotspots with those from surface reflectance during the study period.

2.8. HYbrid Single-Particle Lagrangian Integrated Trajectory (HYSPLIT) Model

The HYSPLIT model was used to investigate complex plume dynamics and vertical wind shear in the atmosphere. HYSPLIT 24-h back-trajectories were computed using the North American Model as a meteorological input, with a 12-km grid resolution. HYSPLIT was run for August 31, 2013 to cover an episode of the Rim Fire to study the complex aerosol transport and dispersion over mountainous terrain during that time (Draxler & Rolph, 2013; Peterson et al., 2014).

2.9. Data Processing for Pairing Datasets in Space and Time

To synchronize the datasets in space and time, hourly averages of some datasets were created. The $PM_{2.5}$ and PBLH from WRF have an hourly time resolution, whereas the AERONET AOD were averaged to a 1-h resolution. This was done with no restrictions on the number of data points (minimum of one data point per one hour) and calculated from the available data points within each hour (counting from 0 to 59 min). Due to the overpass time of satellite products and launch frequency of radiosonde (00:00 UTC), those datasets have a one-daytime measurement per day (potentially two for VIIRS).

A second averaging process was performed to co-locate the AERONET data with DB and MAIAC. Following the commonly used convention, AERONET AOD was averaged over a 30-min window centered at the time of the satellite overpass while the satellite AOD was averaged using a 25 km radius around the AERONET station (Hsu et al., 2019; Loría-Salazar et al., 2016; Sayer, 2020). AERONET AOD was converted from 500 to 550 nm using the AE (Angstrom, 1929; Eck et al., 1999).

The bulk (>95%) of the AERONET AOD was taken from the Level 2 (cloud screened and quality assured) data set. To counter the rare overscreening of highly variable smoke in in this product, Level 1 (unscreened) data were added back to the final data set used during the active fire periods using the fire-filter algorithm of Loría-Salazar et al. (2016).

3. Smoke Height Boundary Layer Ratio (SHBLR)

A first-order approach, which we call the Smoke Height Boundary Layer Ratio (SHBLR), was developed to distinguish whether emitted/transported smoke was likely to reach ground level or was confined to the free troposphere. The SHBLR was determined using the model terrain elevation and PBLH (WRF) in conjunction with the PIHs (MAIAC: Terra and Aqua; ASHE: run without CALIOP, assuming SSA = 0.88). The PBLH for each WRF grid was the mode of the time of each overpass. This was done because multiple points from the satellite retrievals were used to match the WRF grid in the spatial averaging process. This method assumes that the PBLH does not differ significantly within one hour of the satellite overpasses, and that the PBL is well mixed. This assumption would not hold near sunrise and sunset, because the PBL varies significantly over those periods, especially the PBLH. However, the satellite overpass times were within a few hours of local solar noon. For each MAIAC and ASHE product, the PIH was spatially averaged to match the horizontal resolution of the WRF grid. The ASHE product provides the PIH above sea level, so the terrain elevation was subtracted using the WRF terrain height. We defined the SHBLR as follows:

$$\mathrm{SHBLR} = \frac{\mathrm{PIH}}{\mathrm{PBLH}} \tag{1}$$

If the SHBLR is close to or less than 1, it implies that the wildfire smoke plumes were confined within the PBL. A smoke plume in the PBL indicates potential health effects due to smoke exposure because of the vertical mixing throughout the boundary layer. This leads to well-mixed conditions where the smoke emissions lead to a homogeneous distribution of aerosol concentrations from the surface throughout the PBL. If the SHBLR is larger than 1, the smoke plumes that were injected into the free troposphere (i.e., above the PBL) did not necessarily reach ground level. In this case, AOD and surface PM are likely to be less strongly coupled (Loría-Salazar et al., 2017; Pierce et al., 2018).

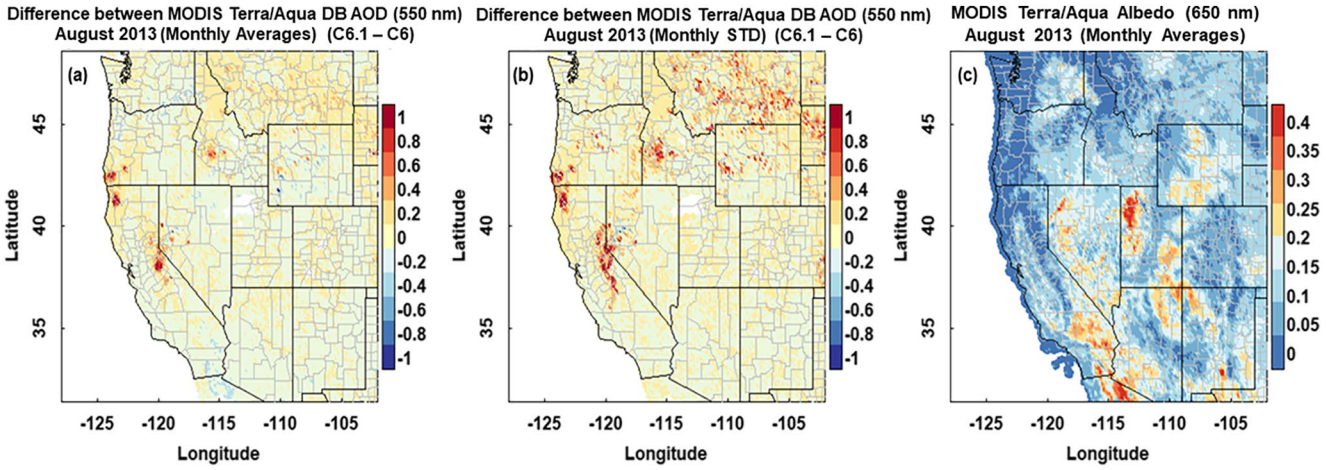

Figure 2. (a) Monthly averages and (b) standard deviations (STD) of the differences in AOD, defined as C6.1 minus C6, between the two MODIS DB versions during August 2013. (c) Monthly average of MODIS surface albedo at 650 nm. AOD, aerosol optical depth; MODIS, MODerate Resolution Imaging Spectroradiometer.

4. Results

4.1. Spatial Distribution and Evaluation of AOD From Ground-Based Sunphotometry and Satellite Retrievals

Figure 1 shows the spatial monthly averages and standard deviation (STD) from DB and MAIAC and from AERONET AOD (circles) during August 2013, and Figure SI.1 shows the location of the fires with respect to the AERONET stations. The monthly averages and STDs of AOD from AERONET remained clean (AOD < 0.1) over areas not affected by smoke, and increased over regions impacted by smoke plumes. For both monthly averages and STDs of satellite retrievals, AOD ranged from ~0.01 to ~0.7. This result indicates potential low aerosol pollution (AOD < 0.1) in the absence of smoke, and regions with poor AQ in the presence of smoke that increased AOD (AOD > 0.5), especially over California, Oregon, Idaho, and Montana. Of the four algorithms, DB from the VIIRS instrument showed the largest AOD hotspots (Figures 1c and 1g) from smoke areas (AOD > 0.5).

Figure 2 shows the differences (C6.1 minus C6) from AOD monthly averages (Figure 2a) and STDs (Figure 2b). For context, a MODIS surface albedo map is provided (Figure 2c) to demonstrate algorithm improvements concerning smoke/cloud discrimination between these two versions related to surface cover (Hsu et al., 2019). For this case, the positive differences from the monthly averages and STDs represents the improvement in the smoke detection algorithm in C6.1 (i.e., less overscreening of variable wildfire smoke as cloud). The negative differences show a reduction of known retrieval artifacts at certain locations (dry lakes and heterogeneous terrain) in the DB AOD algorithm for C6.1, due to incorrect surface reflectance assumptions (Loría-Salazar et al., 2016; Sayer et al., 2019).

Table 1 shows the spatial-temporal statistical summary of AERONET, MODIS DB C6, MODIS DB C6.1, VIIRS DB, and MAIAC AOD during August 2013. For the entire period and at all stations, the AERONET AOD ranged from 0.01 to 2.49. (mean = 0.13, median = 0.08, STD = 0.17), implying high aerosol loading in areas affected by wildfire smoke. The summary statistics for the DB from MODIS were similar to those for AERONET, while those for the DB from VIIRS retrieved higher AOD values compared to AERONET (VIIRS DB AOD = 3.88, AERONET AOD = 2.49). The MAIAC AOD showed less variability than both AERONET and the DB algorithms. The low bias in C6 MAIAC AOD probably resulted from both the lack of a higher absorption smoke aerosol model and the use of the regional background aerosol model for AOD retrievals in the case of detected smoke. The asymmetry of these summary statistics (i.e., means and often standard deviations were larger than the median values) indicate that the overall AOD distribution was skewed: typical low-AOD background conditions, punctuated by periods of elevated aerosol loading from, for example, wildfire smoke.

Table 1
Spatial-Temporal Statistical Summary of AERONET, MODIS DB C6, MODIS DB C6.1, and MAIAC AOD During August 2013, Using 12 AERONET Stations in the Western USA

	AERONET	MODIS DB (C6)	MODIS DB (C6.1)	VIIRSDB	MODISMAIAC
N	3,190	439	431	468	521
Min	0.01	0.02	0.02	0.02	0.02
Max	2.49	2.89	2.32	3.88	1.7
Mean	0.13	0.14	0.13	0.18	0.17
Median	0.08	0.09	0.06	0.07	0.13
Std (±)	0.17	0.24	0.24	0.39	0.19
Percentile25	0.05	0.05	0.03	0.05	0.09
Percentile50	0.08	0.09	0.06	0.07	0.13
Percentile75	0.13	0.16	0.12	0.12	0.2

The list of stations with their respected coordinates is shown in Table SI.1 in the SI. AOD, aerosol optical depth; MAIAC, multi-angle implementation of atmospheric correction; MODIS, MODerate Resolution Imaging Spectroradiometer; VIIRS, Visible Infrared Imaging Radiometer Suite.

Figure 3 shows scatterplots of MODIS AOD retrievals and AERONET AOD over 12 stations; the stations are split either by site (upper row) or into non-fire and fire periods (lower row). Table 2 shows the number of data points (N), normalized mean square error (NMSE), root mean square error (RMSE), and coefficient of determination (r^2), where $r^2 = 1$, RMSE = 0, and NMSE = 0 indicate perfect agreement. The set of equations can be found in the SI (Equation 1–6) of Loría-Salazar et al., (2016). These evaluation metrics are commonly used to evaluate AQ model performance (Appel et al., 2011; Chang & Hanna, 2004; EPA 454/R-08-003, 2008; Loría-Salazar et al., 2016; Simon et al., 2012; Wilkins et al., 2018).

Overall, the C6 MAIAC algorithm presented the lowest NMSE (0.42) and RMSE (0.1) as well as the highest r2 (0.84). DB C6.1 and VIIRS showed a significant improvement with respect to C6 (C6.1: $r^2 = 0.75$, VIIRS: $r^2 = 0.79$, compared to C6: $r^2 = 0.62$). For MODIS C6.1, there was a moderate drop in NMSE and RMSE, and for VIIRS DB, NMSE was higher (1.37), implying that although AOD can capture the spatiotemporal variability of the data, its magnitude was overestimated, at least during this event (Table 2).

4.2. Spatial Assessment of NASA Fire-Related Satellite Products

Figure 4 shows the monthly averages and daily counts of FRP at 1 × 1 km^2 resolution along with their respective histograms during August 2013. As expected, FRP presented lower values during the morning overpass (Terra) than the afternoon overpasses (Aqua, VIIRS). This difference is partially attributed to the change in the dynamics of the atmosphere during the day that impact fire behavior, especially for large wildfires typical in the western USA Similar to the finding from Beck et al. (2002) for Canadian wildfire events as well as other regions of South America, Africa, Australia, and Asia (Giglio, 2007). The numbers of hotspots from fires observed in August 2013 were 6,588 (Terra), 6,378 (Aqua), and 10,166 (VIIRS). The ranges of monthly averaged FRP were 3.6–3,100 W m^{-2} (Terra), 0–4,000 W m^{-2} (Aqua), and 0–2,900 W m^{-2} (VIIRS). There were 68 Terra, 145 Aqua, and 85 VIIRS locations with FRP greater than 200 W m^{-2} (Figures 4g–4i). In general, the results for Aqua MODIS FRP and VIIRS FRP were similar, differing in that VIIRS FRP can provide higher spatial resolution, while Aqua MODIS reports more fires with higher FRP values. The differences are also related to the fact that the MODIS fire count and FRP retrieval sensitivity has a greater viewing zenith angle dependency than VIIRS due to differences in the sensor designs (Li et al., 2018). Aqua MODIS and VIIRS FRP estimates are very comparable in fire clusters, except for large boreal forest fires, where VIIRS FRP is ~47% smaller (Li et al., 2018). Therefore, understanding the similarities and inconsistencies between both datasets are important for accurate AQ applications, especially in CTMs, where FRP is often used to model wildfire emissions, which are used as inputs to CTMs (e.g., Sofiev et al., 2009).

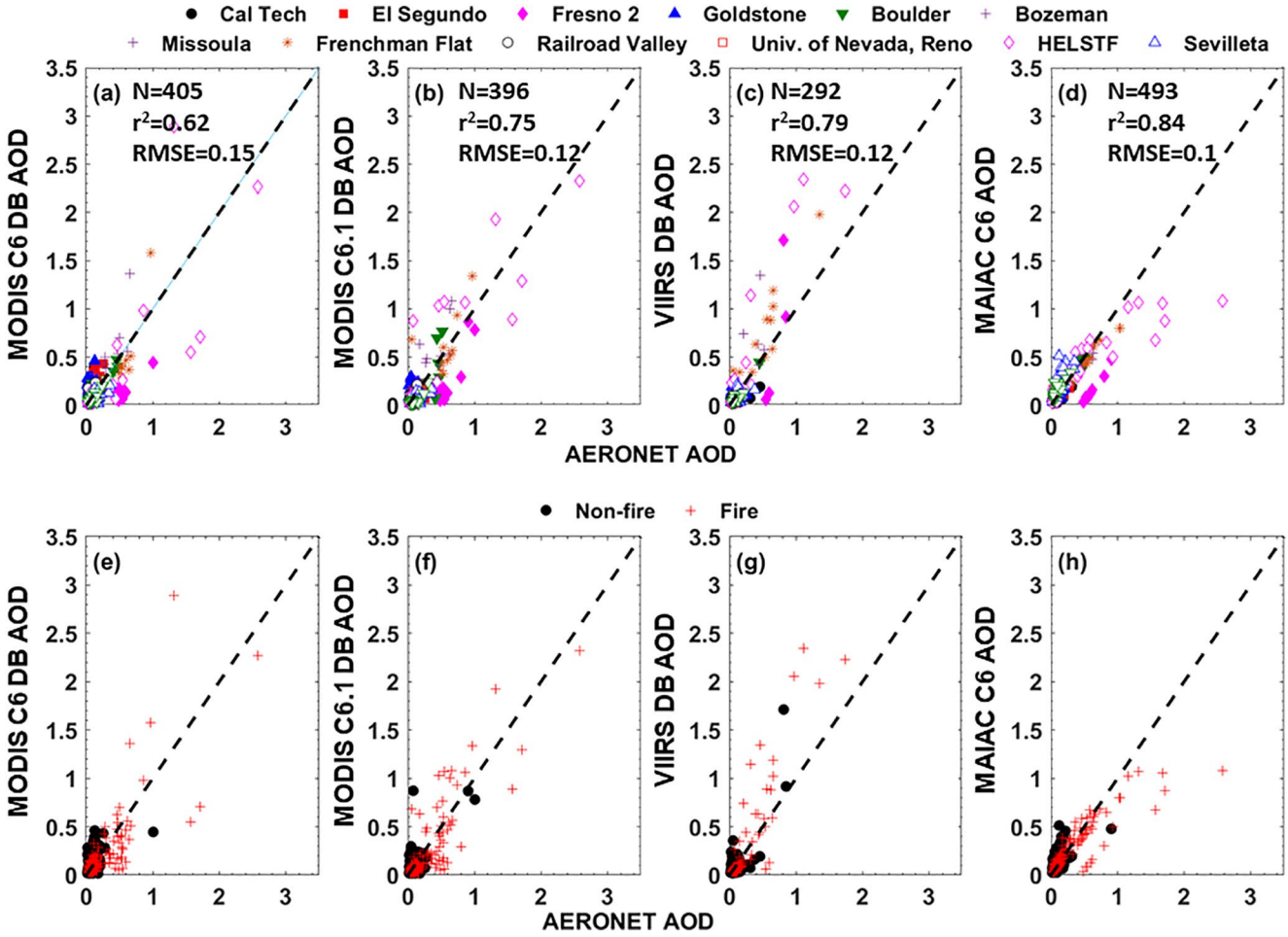

Figure 3. Scatterplots of satellite retrievals of AOD (550 nm) against AERONET AOD (interpolated 550 nm) during August 2013. Top panel, categorized by stations: algorithms for (a) Deep Blue (DB) MODIS C6, (b) DB Col. MODIS 6.1, (c) DB VIIRS, and (d) MODIS MAIAC. Bottom panel, categorized by fire and non-fire periods:algorithms for (e) DB MODIS C6, (f) DB Col. MODIS 6.1, (g) DB VIIRS, (h) MODIS MAIAC. Dashed line: the 1:1 line. Evaluation metrics such as N, r^2, and RMSE are associated to the entire spatial temporal domain, therefore, the evaluation metrics on (e–h) are the same than (a–d). AOD, aerosol optical depth; MAIAC, multi-angle implementation of atmospheric correction; MODIS, MODerate Resolution Imaging Spectroradiometer; RMSE, root mean square error; VIIRS, Visible Infrared Imaging Radiometer Suite.

Table 2
Spatial-Temporal Statistical Evaluation of MODIS DB C6, MODIS DB C6.1, VIIRS DB, and MODIS MAIAC AOD During August 2013 Against AERONET. The AERONET Stations Selected had at Least 70% Temporal Coverage with Respect to the AOD Satellite Retrievals

	MODIS DB (C6)	MODIS DB (C6.1)	VIIRS DB	MODISMAIAC
N pairs	405	396	292	493
NMSE	1.13	0.79	1.37	0.42
RMSE	0.15	0.12	0.12	0.1
r^2	0.62	0.75	0.79	0.84

AOD, aerosol optical depth; MAIAC, multi-angle implementation of atmospheric correction; MODIS, MODerate Resolution Imaging Spectroradiometer; NMSE, normalized mean square error; RMSE, root mean square error; VIIRS, Visible Infrared Imaging Radiometer Suite.

The C6 DB AOD algorithm was previously reported to overscreen spatially variable smoke plumes in this region (Loría-Salazar et al., 2016). However, the AOD retrievals from DB C6.1 and VIIRS seemed to have reduced this problem. Here, the DB and VIIRS retrievals had generally higher AOD hotspots compared to MAIAC. There was also an AOD hotspot in the MAIAC AOD algorithm that was close to the edge of the Great Salt Lake along the Utah-Nevada border (Figure 1c), which did not appear to be associated with an FRP hotspot (Figures 4a–4c). We suggest that the hotspot is likely because there are known difficulties in the representation of ephemeral water bodies and mixed pixels in the land mask used, leading to artificial hotspots in AOD retrieval algorithms (Carroll et al., 2017). Finally, multiple low-intensity fires in Arizona, New Mexico, and Colorado did not noticeably increase monthly averages or STDs of AOD in any algorithm (Figures 4a–4c), but they were represented by a slightly elevated AERONET monthly average AOD (Figure 1).

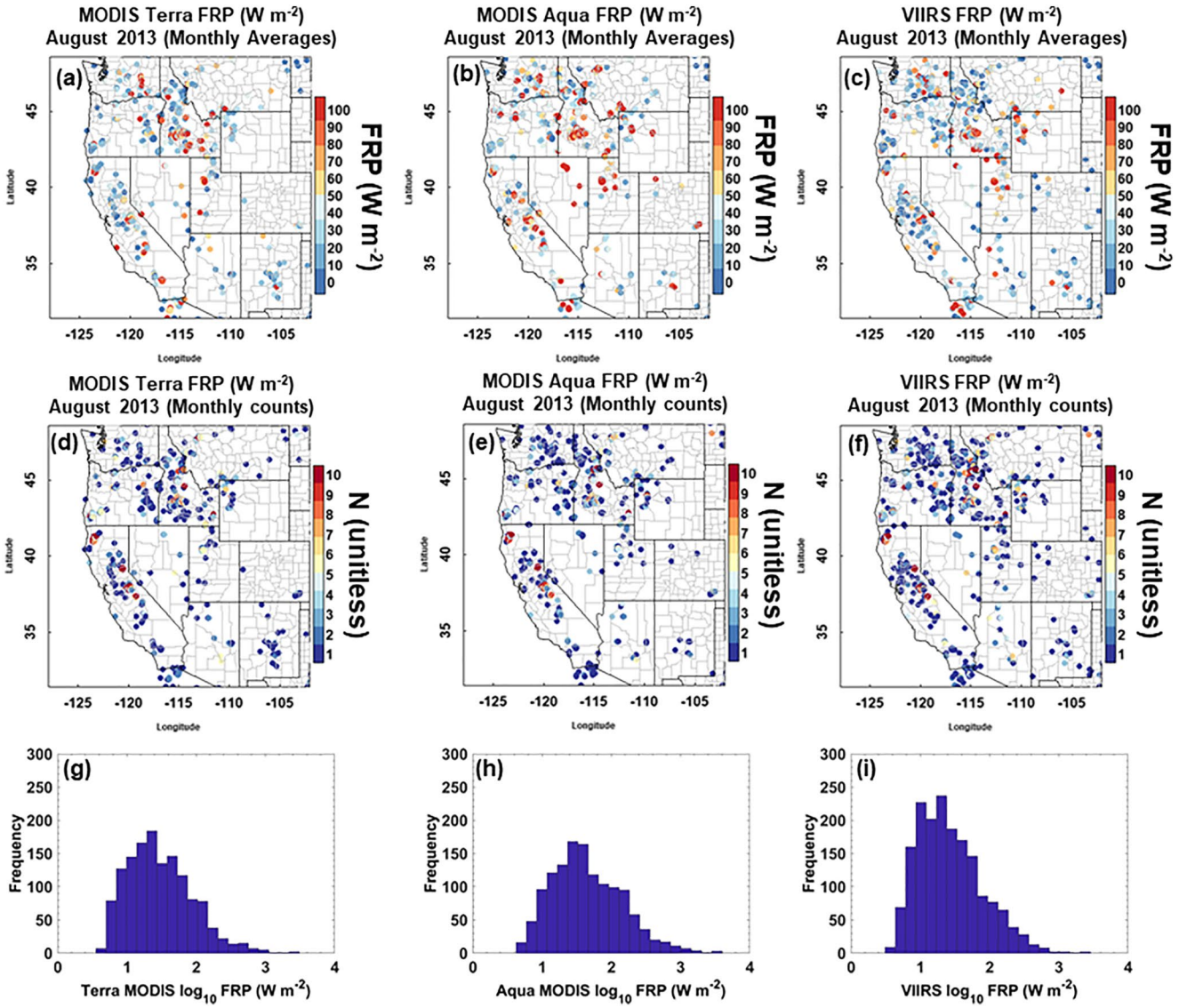

Figure 4. Spatial distribution of FRP (W m^{-2}) in August 2013. (a–c) Monthly averages for Terra MODIS, Aqua MODIS, and VIIRS at one × 1 km^2 resolution. (d–f) Data point counts for MODIS Terra, MODIS Aqua, VIIRS at 1 × 1 km^2 resolution. (g–i) Frequency histograms of log_{10} FRP for MODIS Terra, MODIS Aqua, VIIRS. MODIS, MODerate Resolution Imaging Spectroradiometer; VIIRS, Visible Infrared Imaging Radiometer Suite.

5. Wildfire Smoke Case Studies

Case studies from August 2013 where ground-based stations and lidar data were available are presented. Three case studies were selected to evaluate the capabilities and limitations of satellite passive remote-sensing products during burning events: (a) the Central California fires (Yosemite Rim and American River Fires), where surface concentrations and complicated transport aloft were observed because of the effect of irregular terrain on the deep-convective PBL; (b) fires on the border of Oregon and California, where heterogeneous aerosol profiles were found under shallow PBL conditions; and (c) an evaluation of the smoke PIH retrievals, which compares the fires described in (a) and (b) and CALIOP retrievals.

5.1. Case Study 1: Yosemite Rim and American River Fires

These massive wildfire events in 2013 started on August 11 (American River; hereafter River) and August 17 (Yosemite Rim; hereafter Rim), and burned 22,407 acres and 257,314 acres, respectively. Information

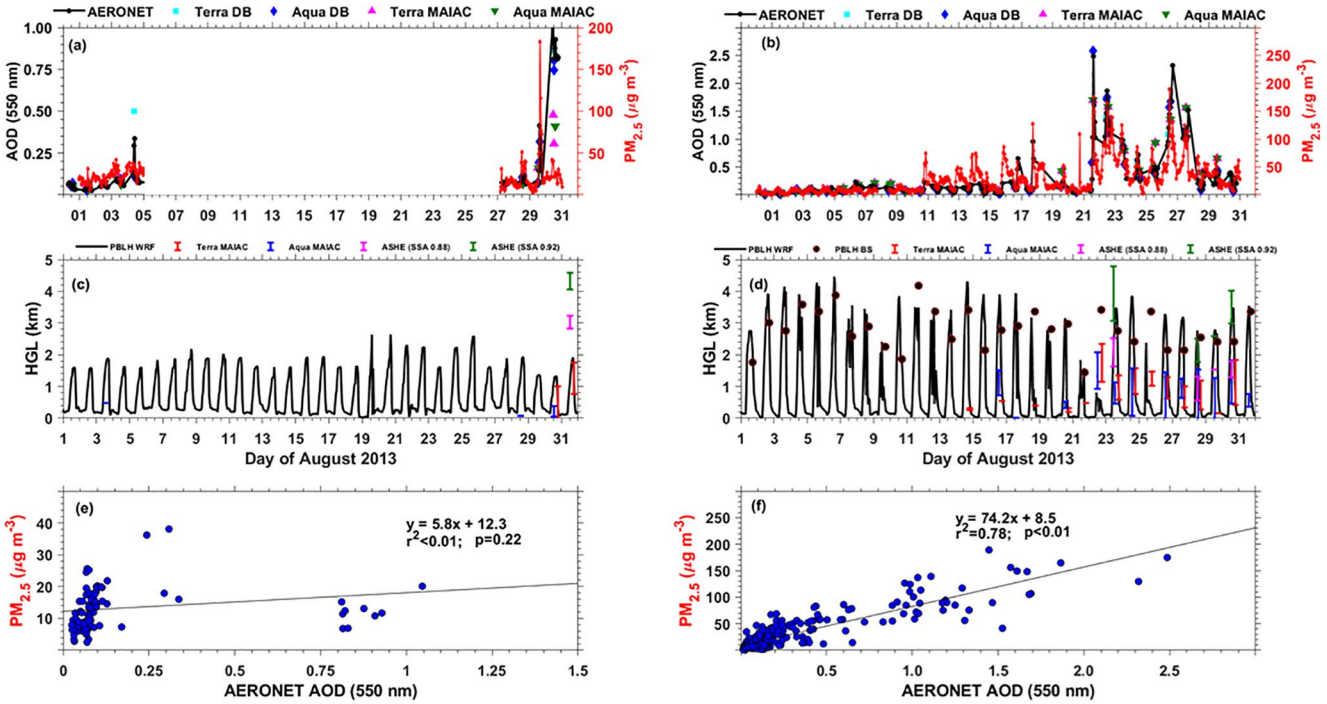

Figure 5. Surface $PM_{2.5}$ mass concentrations, AOD from AERONET, and satellite-derived products over Fresno, CA, and Reno, NV, during August 2013. Hourly variability of AOD (left axis) and $PM_{2.5}$ (right axis) concentrations over (a) Fresno and (b) Reno. Comparison of PIH products height above ground-level (HGL) between MAIAC and ASHE with WRF outputs of PBLH over (c) Fresno and (d) Reno, with additional balloon sounding (BS) PBLH. Middle of error bars: average; length: variability. Scatterplot with regression equation of AERONET AOD and $PM_{2.5}$ over (e) Fresno and (b) Reno. AOD, aerosol optical depth; ASHE, aerosol single scattering albedo and layer height estimation; MAIAC, multi-angle implementation of atmospheric correction; PBLH, planetary boundary layer height; PIH, plume injection height; PM, particulate matter; WRF, Weather Research and Forecasting.

on field experiments and modeling related to the Yosemite Rim Fire can be found in Peterson et al. (2014), Yates et al. (2016), and Baker et al. (2018). Smoke from these fires was observed using two AERONET stations (Fresno 2 and University of Nevada, Reno) and two $PM_{2.5}$ monitoring stations from the EPA (one co-located with the Fresno 2 site, and the other about 1 km away from the University of Nevada, Reno site). The AOD and $PM_{2.5}$ concentrations in both locations provided information about aerosol transport over the complex terrain.

Figure 5 shows the hourly AERONET AODs, daily MODIS AODs, and surface $PM_{2.5}$ concentrations and scatterplots over Fresno (Figures 5a and 5c) and Reno (Figures 5b and 5f) during August 2013. Also shown is the hourly variability of PBLH using WRF, and daily variability of PBLH calculated from the balloon sounding (in Reno) with the daily retrieval of PIH from MAIAC and ASHE (Figures 5c and 5d). Over Reno (Figures 5b, 5d, and 5f), AOD and $PM_{2.5}$ were strongly temporally correlated ($r^2 = 0.78$). This correlation implies that most of the smoke transported from the Yosemite Rim and American River Fires to Reno was confined within the PBL, where the smoke aerosols were mixed down to the surface. All the PIH products showed that most of the plumes were confined within the PBL (Figure 5d). The ASHE products presented higher PIH than the MAIAC retrievals. The differences between MAIAC and ASHE PIH results may be because the MAIAC algorithm is not recommended for use beyond ±75–150 km downwind of the main source of the fire, where the thermal contrast technique is less reliable (Lyapustin et al., 2020).

Over Fresno (Figures 5a, 5c, and 5e), the AOD and $PM_{2.5}$ were not correlated ($r^2 < 0.01$) and there were few retrievals from the PIH products. However, the spike in AOD and lower values of surface $PM_{2.5}$ on August 31 were captured in the ASHE PIH (Figure 5c). The ASHE retrievals placed the smoke aerosols above the PBL, signifying that they were not entrained into the PBL and therefore not able to mix down to the surface. These results provide evidence that complicated aerosol transport affected the vertical distribution of

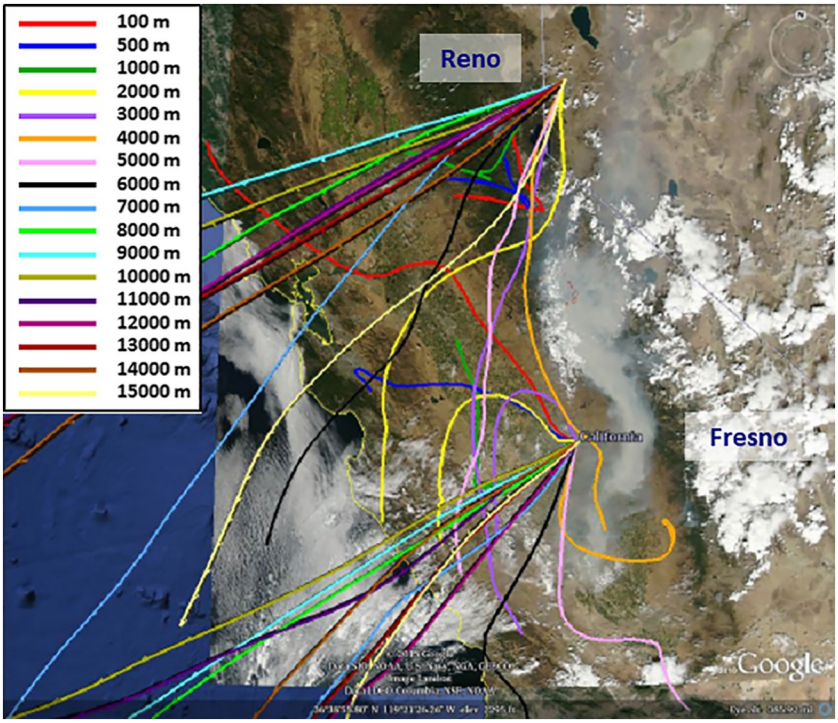

Figure 6. HYSPLIT 24-h back-trajectories (100–15,000 m) from the North American Model (NAM) at 12-km resolution at Fresno, CA, and Reno, NV, on August 31, 2013, superimposed onto a MODIS Aqua true-color image from NASA World View (https://worldview.earthdata.nasa.gov). MODIS, MODerate Resolution Imaging Spectroradiometer.

aerosol concentrations in the atmospheric column. This was evident when aerosols were present at higher elevations but the surface concentrations remained low.

To investigate the vertical distribution of aerosol concentrations downwind of the Rim Fire, we used HYSPLIT 24-h back-trajectories using the North American Mesoscale model. HYPSLIT trajectories from Fresno and Reno on August 31, 2013 are shown in Figure 6 with a NASA World View MODIS visible image of the smoke plume from the Rim Fire. Over Reno, the back-trajectory analysis revealed that the low-level trajectories (100 and 500 m) crossed the smoke plumes, bringing aerosols into the PBL. The majority of the upper-level trajectories over Reno came from areas without smoke plumes; however, the 2,000 and 4,000 m trajectories passed over the smoke plume, bringing in aerosols at multiple levels in the atmosphere. Meanwhile over Fresno, the low-level trajectories (100 and 500 m) came from the north over the Central Valley (i.e., region without wildfire smoke). While the upper-level trajectories crossed the smoke plume from the Rim Fire (4,000 and 5,000 m). Creating a heterogeneous vertical distribution of aerosol pollution in the atmosphere above Fresno.

In addition to this case study in Reno and Fresno, two other sites in California were used to evaluate the scope and limitations of the PIH satellite retrievals against ground-based total attenuated backscattering lidar data: Dodge Ridge Ski Resort on August 23 and Donell Vista on August 29. Because of the spatial resolution difference between ASHE and MAIAC products, MAIAC retrievals were expected to have more variability than the ASHE products. Results from the satellite-derived PIH are shown in Figures 7b and 7c. Visual inspection of images from NASA World View suggested no cloud cover in any of the locations during the satellite overpasses. This visual inspection was performed because clouds can be misclassified as smoke from fires.

During August 23, most of the aerosols were confined within the PBL (Figure 7b). MODIS and VIIRS ASHE (assuming SSA = 0.88) and MAIAC retrievals were able to capture the PIH well in comparison to the lidar data (~2 km AGL). In contrast, the ASHE product (assuming SSA = 0.92) resulted in higher PIH retrievals. These results are consistent with those of Lee et al. (2015), who found SSA values for wildfire smoke over

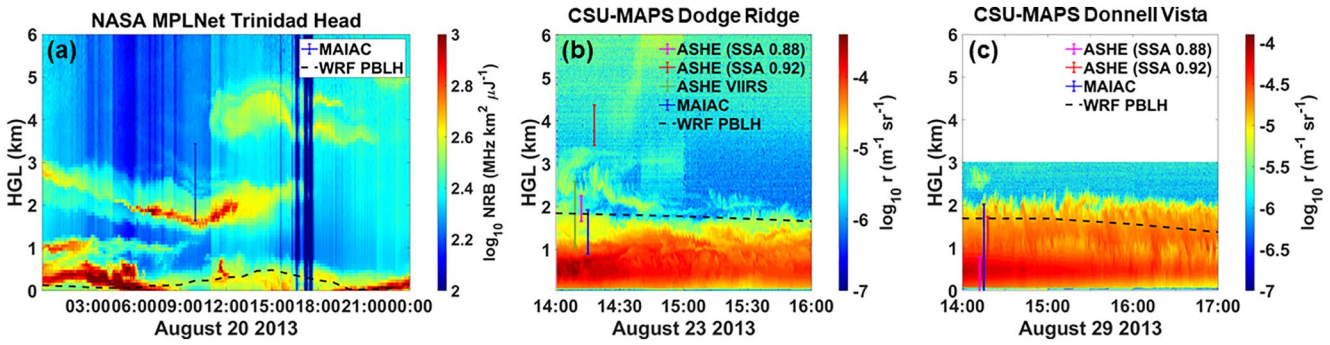

Figure 7. Backscattering vertical cross-section (r) using ground-based lidar and comparison with PIH from MODIS and VIIRS ASHE and MODIS MAIAC products. Dashed lines: PBLH using WRF outputs. Middle of error bars: average; length: standard deviation. (a) Aerosol backscattering from Trinidad Head, CA, NASA MPLNET station on August 20, 2013. Total attenuated backscattering from (b) Dodge Ridge Ski Resort, CA, August 23, 2013, and (c) Donnell Vista, CA, August 29, 2013 from CSU-MAPS. The error bar represents the standard deviation, and the middle is the mean. Although all satellite PIH data represent observations at the same time (all coming from the Aqua overpass in b and c), they are slightly offset to help distinguish differences between them. ASHE, aerosol single scattering albedo and layer height estimation; MAIAC, multi-angle implementation of atmospheric correction; MODIS, MODerate Resolution Imaging Spectroradiometer; PBLH, planetary boundary layer height; PIH, plume injection height; VIIRS, Visible Infrared Imaging Radiometer Suite; WRF, Weather Research and Forecasting.

the western USA ranging from 0.87 to 0.93. The choices of SSA = 0.88 and SSA = 0.92 can serve to provide typical lower and upper bounds of the uncertainty range of the plume height (SSA assumptions are the primary source of uncertainty). The ASHE retrievals when SSA = 0.92 were closer to a weaker aerosol layer (lower backscattering signal) seen by the lidar above the PBLH (3–4 km AGL). In this case, it was expected that the ASHE retrievals be closer to the top of the optically thick (i.e., lower) aerosol layer, given an appropriate SSA.

On August 29, the aerosol coming from the fire remained within a well-mixed atmospheric boundary layer for most of the study period. Toward the end (5:00 p.m. local time), the PBLH started to decrease due to the decreased surface sensible heat flux associated with less incoming solar radiation. This atmospheric process allowed aerosols to reach levels above the PBLH. The aerosol pollution had a less homogeneous vertical distribution than on August 23, challenging the satellite retrievals, (Yates et al., 2016, Figure 3). Although ASHE and MAIAC retrievals, on average, captured a deep-lower aerosol layer (~500 m AGL), the height of the plume (~2 km AGL) was also captured within the variability of the retrievals (Figure 7c, error bars).

5.2. Case Study 2: Border of California and Oregon Fires

Multiple wildfires were captured during August 2013 on the border of Oregon and California (Figures 1b–1d). On August 20, aerosol backscattering data from the Trinidad Head MPLNET lidar station captured complicated vertical aerosol transport from the fires. Figure 7a shows the backscattering signal from the Trinidad Head MPLNET lidar station and the Terra MAIAC PIH. There was agreement between the lidar and MAIAC PIH in the plume height aloft (~2.5 km AGL). Therefore, the plume above the PBL was captured by MAIAC, implying transport of aerosols aloft due to the intensity of the fire injecting smoke plume above the PBL. During the morning of August 20, in the initial PBL development, the smoke from the fires penetrated the free troposphere because the PBL inversion cap was not strong enough to trap the smoke. The smoke can be related to emissions from the previous day which penetrated the free troposphere during the nocturnal and stable boundary layer. In the afternoon, a well-mixed boundary layer due to convection was able to capture smoke near ground-level (<500 m), but independent layers of smoke aloft were also found.

The MAIAC PIH estimates over the Trinidad Head AERONET station (Figure 8b) were at higher altitude than the PBLH from WRF. There was no correlation between AERONET AOD and surface $PM_{2.5}$ (Figure 8c), implying heterogeneous vertical mixing due to the smoke from the fires, which agreed with MAIAC PIH retrievals within the average±STD. No ASHE PIH retrievals were found around the AERONET station at Trinidad Head.

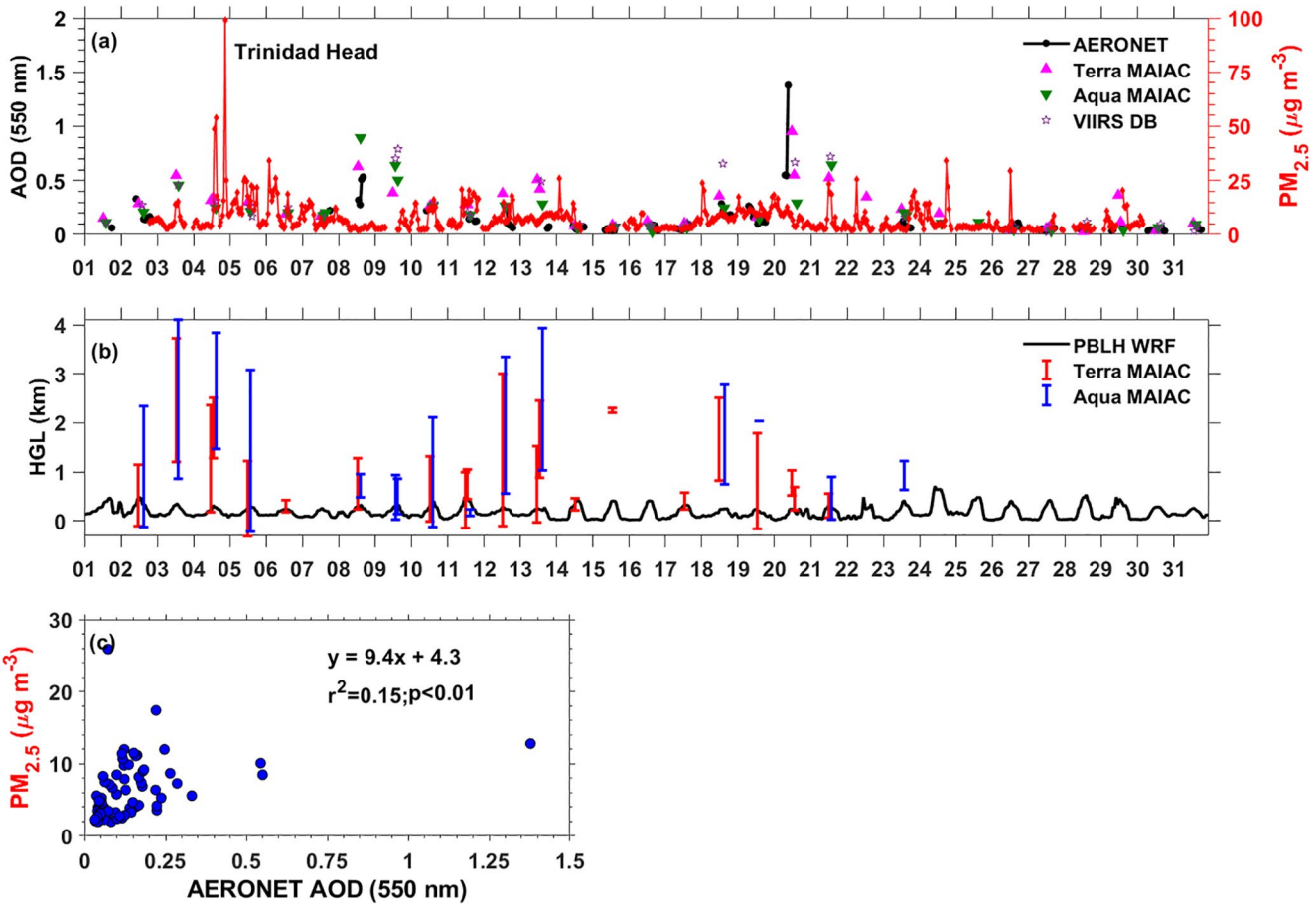

Figure 8. Representation of complicated aerosol transport using surface $PM_{2.5}$ mass concentrations, AOD from AERONET, and satellite-derived products over Trinidad Head, CA, during August 2013. (a) Hourly variability of concentrations of AOD (left axis) and $PM_{2.5}$ (right axis). (b) Comparison between PIH products from Terra MAIAC and Aqua MAIAC and WRF outputs of PBLH. Middle of error bar: average of the PIH datasets; length: standard deviation. Fig(c) Scatterplot with regression equation of AERONET AOD and $PM_{2.5}$. AOD, aerosol optical depth; MAIAC, multi-angle implementation of atmospheric correction; PBLH, planetary boundary layer height; PIH, plume injection height; PM, particulate matter.

5.3. Case Study 3: Evaluation of PIH Retrievals Using CALIOP Lidar Retrievals

Figure 9a shows the average height of the total attenuated light scattering signal of each CALIPSO overpass over the western USA during August 2013. CALIPSO overpassed the border of the Oregon and California fire on August 15 (Figure 9b) and near the Yosemite Rim Fire on August 26 (Figure 9e). Smoke plumes transported from the different sources in California, Oregon, and Idaho are shown for August 23 (Figure 9d) and August 25 (Figure 9c). MAIAC PIH was able to capture PIHs within the observed variability for the August 15 case (Figure 9b) because of its proximity to the fire. For the other cases (Figures 9c–9e), MAIAC PIH decreased, possibly because the smoke plumes were more than 100 km from the fire so the algorithm is more uncertain. ASHE retrievals from VIIRS agreed (averages±STDs) with CALIOP on August 25 (Figure 9c); however, results were limited for August 23 (Figure 9d) and August 26 (Figure 9e). CALIOP retrievals showed aerosols above the PBL derived from WRF. This finding agreed with the complicated vertical distribution found in Case Studies 1 and 2.

6. Discussion of the Scope and Limitations of Novel Satellite-Derived Smoke Products and Recommendations for AQ Modeling

The ASHE PIH product (Figure 10a) had fewer daily data points because it had lower spatial resolution than the MAIAC algorithm. However, it is still possible to identify areas where aerosol pollution from wildfire smoke affected ground-level $PM_{2.5}$ concentrations using ASHE. Terra and Aqua MAIAC retrievals were

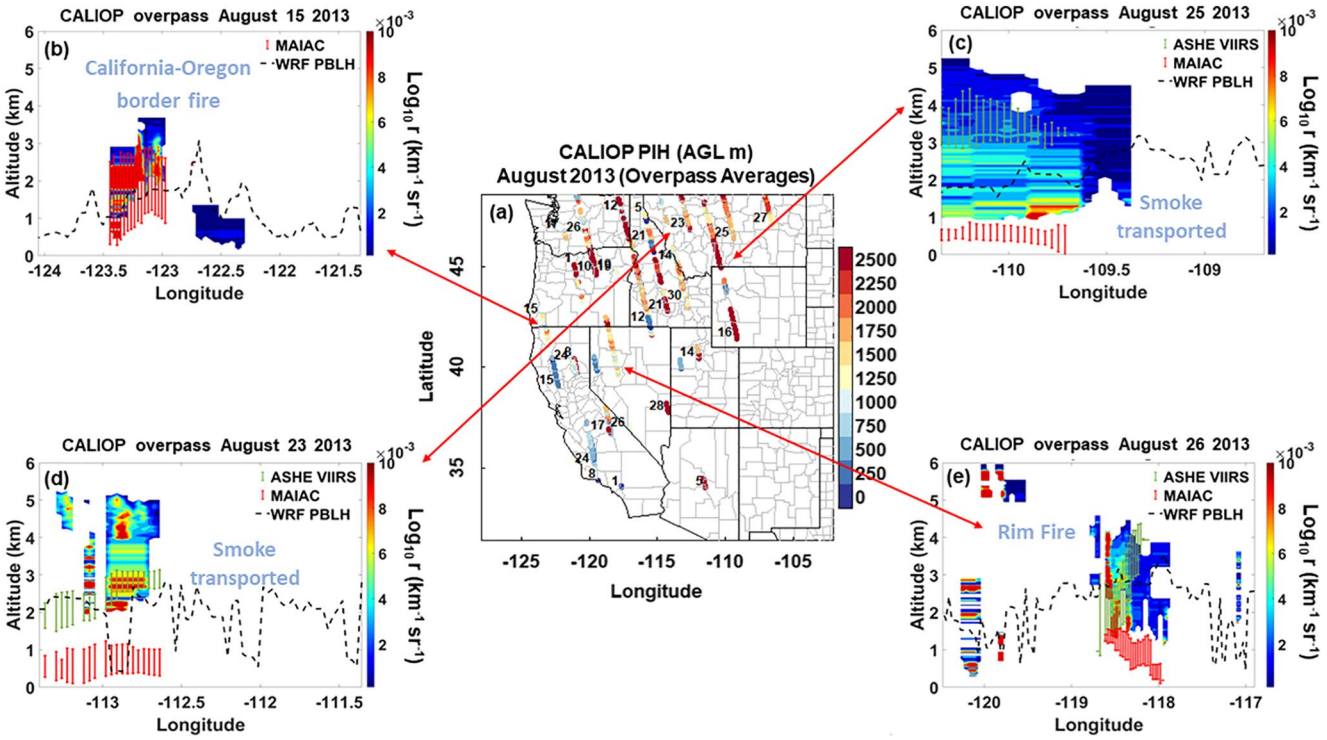

Figure 9. Comparison between PIH algorithms and CALIOP total attenuated backscattering (r) retrievals. (a) Average height of CALIOP backscattering retrievals. (b) Comparison of PIH products over the California-Oregon border fires. (c and d) Comparison of PIH from smoke transported from the Yosemite Rim fire and Idaho fires. (e) Comparison of PIH from smoke transported from the Yosemite Rim fire. CALIOP, cloud-aerosol lidar with orthogonal polarization; PIH, plume injection height.

separated to recognize the differences in aerosol transport and injection mechanisms during the morning and afternoon overpasses. This was done to investigate the atmospheric processes driving the transport of the plumes within the PBL and in the atmosphere aloft.

During the morning overpass (Figures 10d–10f), more aerosols were above the PBL (i.e., SHBLR > 1), leading to less mixing of aerosols down to the surface. This was because PBLH was, on average, significantly lower during the morning overpass (Figure 10d) compared to the afternoon overpass (Figures 10a and 10g). This pattern is typical of diurnal PBL development caused by increased turbulence in the afternoon from solar heating of the Earth's surface. The percentage of aerosols confined within the PBL was higher during the afternoon overpasses (ASHE: Figure 10b; MAIAC Aqua: Figure 10h) than during the morning (MAIAC Terra: Figure 10e).

One key example of the role of smoke in the PBL can be explored based on smoke from the fires near the border between California and Oregon using data from the Trinidad Head, CA station. During the morning (Figure 10e), the PBLH was, on average, less than 1,000 m, but in the afternoon (Figures 10b and 10h), the same area had an average PBLH up to 1,750 m. Aerosol confinement during the morning (Figure 10f) was significantly lower than in the afternoon (Figures 8a, 10c, 10c and 10i). This behavior was captured by the SHBLR, which was ~15 during the morning and decreased to ~2 during the afternoon on August 20 at the Trinidad Head, CA station (Figure 7a, lidar data show the multiple smoke layers and smoke diurnal distribution) where AOD was >0.2 but the surface pollution did not increase ($PM_{2.5}$<25 μg m^{-3}), as shown in Figure 8a. A combination of atmospheric and fuel conditions during the afternoon enhanced the intensity of the fire, creating higher smoke plume injection heights above the PBL and into the free troposphere. This phenomenon was captured by MAIAC and ASHE. However, the increase in temperature and water vapor released (latent heat) by the fire also created feedbacks to the atmosphere and may have enhanced the depth of the PBL. The same phenomenon also occurred for the 2013 Yosemite Rim Fire, with smoke at multiple layers of the atmosphere transported from the Yosemite Rim Fire to Reno (AOD < 0.2, $PM_{2.5}$ < 25 μg m^{-3})

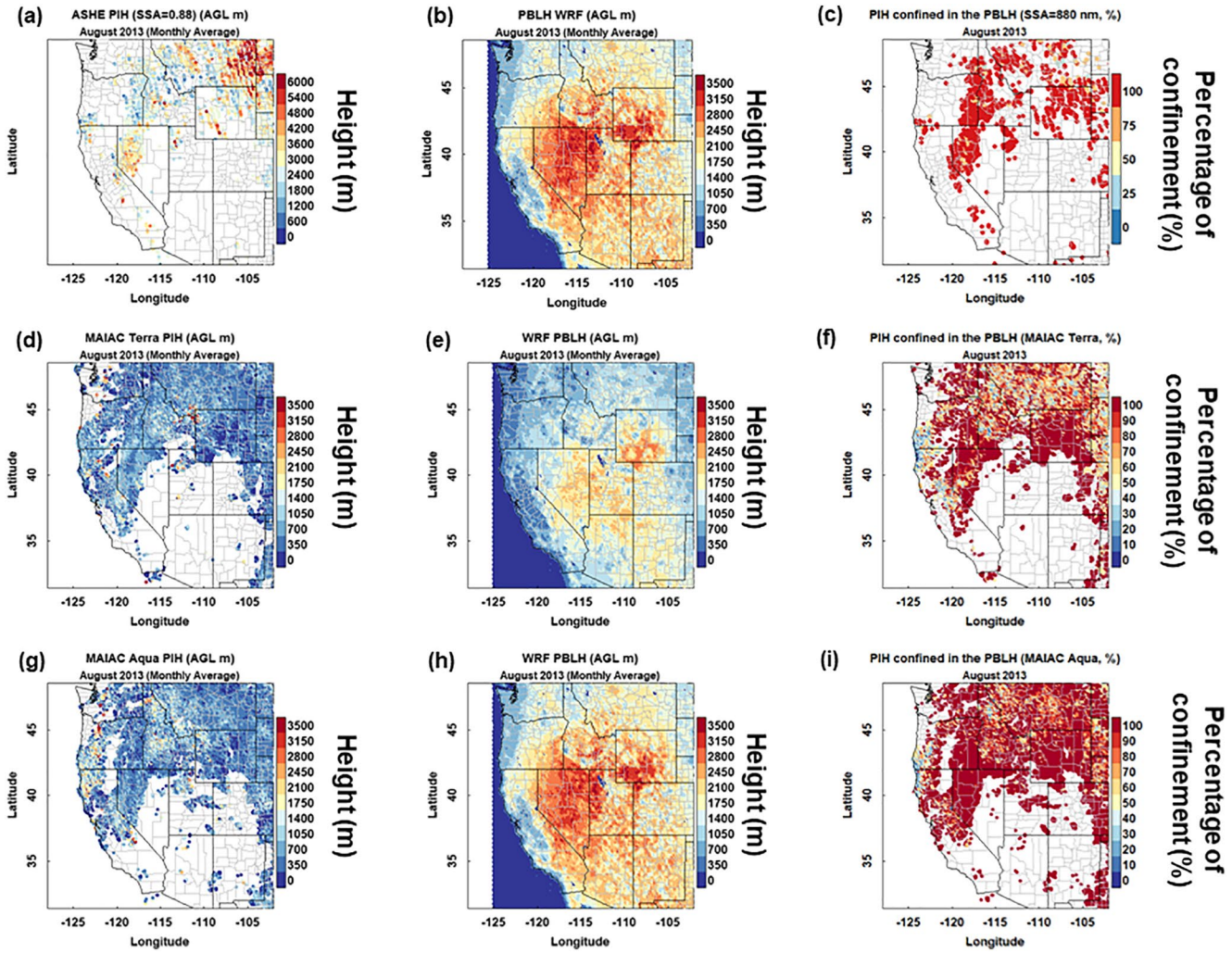

Figure 10. Data used to calculate the percentage of confinement of near-surface aerosol pollution for ASHE over the western U.S. during August 2013. (a, d, and g) PIHs from MAIAC and ASHE (SSA = 0.88) spatially averaged to match the WRF PBLH output. (b, e, and h) Monthly averages of WRF ABLH synchronized with MAIAC and ASHE PIHs. (c, f, and i) Percentage of occasions when the smoke plumes were found within the PBLH for MAIAC and ASHE. ASHE, aerosol single scattering albedo and layer height estimation; MAIAC, multi-angle implementation of atmospheric correction; PBLH, planetary boundary layer height; PIH, plume injection height; SSA, single scattering albedo; WRF, Weather Research and Forecasting.

and Fresno (AOD>0.2, $PM_{2.5}$<25 μg m^{-3}), where SHBLR~0.22 and SHBLR~1.33, respectively on August 31 (Figure 7). The increasing PBLH due to the fire feedbacks can lead to confining the aerosol pollution within the PBL instead of smoke plume injection heights above the PBL. The higher PBLH due to the presence of smoke has been reported in model results due to the absorption component of aerosols impacting the PBL physics (Li et al., 2017, 2018, 2019).

The relationship between PBLH and PIH is important for aerosol vertical distribution and transport. When a fire grows and intensifies, it can create higher smoke plume injection heights due to the increased buoyancy and sensible heat flux. The resulting smoke plumes may still be capped by the boundary layer because of the atmospheric conditions during the burn (e.g., stable atmosphere vs. unstable atmosphere). Resultsfrom ASHE were similar to the ones from MAIAC with lower spatial-temporal resolution due to the combination of the instruments used, OMI and MODIS. However, with the MAIAC higher spatial-temporal resolution product, it is possible to diagnose when ground-level AQ is affected by aerosol pollution during the fire events in August 2013 near the fire sources.

If the SHBLR is implemented in models these, it will likely be possible to improve estimates of wildfire smoke exposure for health effects studies. CALIOP retrievals have the potential to vertically resolve information

about the PBLH and aerosol height. However, the availability of quality level 2 CALIOP retrievals for AQ modeling purposes is limited by lidar signal-to-noise ratios, extinction of the lidar signal, obstruction by clouds, and geographical separation between successive orbital paths (see stripes of CALIPSO; Figures 9 and SI.24–SI.S28 compared to Figures 10a, 10d, and 10g). The novelty of the ASHE and MAIAC products are largely due to their improved spatial-temporal resolution with respect to other NASA algorithms for PIH, such as the CALIOP instrument (once every 16 days sub-spacecraft coverage) as well as MISR MINX (once every 9 days global coverage) (Cheeseman et al., 2020; Kahn et al., 2007; Winker et al., 2010).

Some limitations can be expected if the SHBLR is incorporated into AQ modeling and exposure studies. However, the SHBLR can be used as a first-order qualitative way to assess the potential impact of smoke on ground-level pollutant concentrations. Uncertainties related to modeled PBLH and the PIH retrievals can affect the accuracy of the SHBLR. More studies and approximations are needed to develop a more quantitative metric to estimate the amount of aerosol pollution confined within the PBL from wildfire smoke plumes and the associated estimates of human smoke exposure.

The ASHE and MAIAC PIH datasets are complementary. The PIH from ASHE can provide daily plume height information both near the source and as the plume is transported downwind. ASHE PIH comes at a comparatively lower resolution and only where there is overlap between the required sensor pairs (i.e., MODIS and OMI, VIIRS, and OMPS). MAIAC provides reliable PIH only near active fires, although at high resolution and for the entire MODIS swath (Cheeseman et al., 2020). More importantly, both ASHE and MAIAC PIHs can be used to improve the vertical wildfire smoke emissions estimates used as inputs to CTMs. This is similar to existing fire emissions inventories that use FRP, and/or surface heat flux, to estimate smoke plume rise (Brey et al., 2018). It is expected that the PIH products would provide better characterization of the vertical profile of smoke concentrations and could improve the exiting FRP plume rise methods. An additional benefit to PIH is the extended horizontal resolution compared to the FRP by capturing more smoke pixels, because the PIH characterizes the smoke behavior (smoke pixels) and not fire behavior (fire pixels). Therefore, PIH could be incorporated into statistical AQ models that aim to estimate smoke concentrations downwind of wildfires, especially the ASHE PIH products at further distances downwind.

Wilkins et al. (2020) showed that a redistribution of the vertical PIHs, with part of the emissions above the boundary layer, led to a reduction of model-predicted surface ozone and an increase in downwind transport. Their study used a CTM with a satellite-based high-altitude injection algorithm and inventory (Peterson et al., 2017) to investigate the effects of major western USA wildfires on a midwestern USA city (St. Louis) in August 2013. Wilkins et al. (2020) concluded that up to 60% of the smoke plumes from those western USA fires were above the 3.5 km layer (model determined PBLH), resulting in downwind ozone concentrations in St. Louis that were increased by 10–80 ppbv. The portion of the smoke that is injected above the PBL is critical to the CTM performance, because it can later be mixed down to the surface and lead to AQ exceedances in locations significantly downwind of the fire (Wilkins et al., 2018, 2020). This demonstrates that reliable satellite-based PIHs can be critical to improving the performance of CTMs modeling the AQ associated with wildfire smoke. In this investigation, we illustrate the importance of incorporating PBL data along with satellite products to investigate the pollutant mixing, and vertical distribution of aerosol concentrations associated with wildfire smoke. AQ studies must have high-resolution PBL inputs during large fire events, especially related to PBL characterization, to obtain better estimates of SHBLR. A similar finding was also found by Cheeseman et al., (2020).

7. Summary

The goal of this investigation was to evaluate satellite AOD and PIH products with the aim of using them as model inputs to estimate the impact of smoke from wildfires on surface-level aerosol pollution. We incorporated a combination of ground-based observations (columnar aerosol loading, $PM_{2.5}$ concentrations, and aerosol vertical distribution) and satellite observations (columnar aerosol loading, smoke plume height, fire intensity, and aerosol vertical distribution) as well as modeled PBL for wildfires events in the western USA during August 2013. We found that:

1. The spatial-temporal statistical evaluation of satellite AOD showed that the MAIAC algorithm presented the lowest normalized mean squared error (NMSE = 0.66), lowest root mean square error (0.1), and highest coefficient of determination ($r^2 = 0.84$). The C6.1 and VIIRS Deep Blue products showed significant improvement over the previous version C6 (C6.1: $r^2 = 0.75$; C6: $r^2 = 0.62$; VIIRS: $r^2 = 0.79$).
2. VIIRS FRP provided a higher spatial resolution, but Aqua MODIS reported more fires with higher FRP values. This is due in part to differences in the across-track sensitivity of the instruments as discussed by Li et al., (2018). Understanding the resemblances and inconsistencies of both datasets is important because FRP retrievals are used in wildfire emission inventories.
3. The hourly variability of AOD and $PM_{2.5}$ during the 2013 Yosemite Rim Fire showed that AOD and $PM_{2.5}$ increased together over Reno, NV ($r^2 = 0.78$), and transport aloft was found on Fresno, CA (i.e., AOD and $PM_{2.5}$ did not always increase together; $r^2 = 0.01$). These results and HYSPLIT back-trajectory analysis suggest that complicated aerosol transport occurred over the Sierra Nevada Mountains, impacting the vertical distribution of aerosol concentrations.
4. By combining PIH and PBLH a Smoke Height Boundary Layer Ratio (SHBLR) was created, a simple metric to express whether aerosols are confined within the boundary layer. Based on the SHBLR, we found that differences in diel meteorological conditions affected the percentage of confinement of the smoke plumes within the PBL. These results can help to improve wildfire smoke exposure estimates for use in health effects studies and to formulate new satellite missions related to AQ and aerosol impacts on climate change (e.g., TEMPO; Zoogman et al., 2017).
5. The smoke from the 2013 Yosemite Rim Fire was transported near ground level to Reno (e.g., SHBLR∼0.22 on August 31). Meanwhile, over Fresno (SHBLR∼1.33 on August 31), elevated aerosol injection heights and smoke transport aloft in the free atmosphere above the PBL kept low concentrations of aerosol pollution at the surface and high concentrations of aerosols aloft. These results agree with those from multiple ground-based stations and lidar stations. For August 20 in the Trinidad Head, CA, MPLNET site, the SHBLR was ∼15, implying complex smoke transport aloft. Ground-based measurements confirmed this result.

We conclude that the Deep Blue C6.1 and VIIRS algorithms for retrieving aerosol pollution due to fire activity in the western USA have significantly improved on the previously identified limitations of this product (e.g., Boehmler et al., 2018; Huang et al., 2021; Loría-Salazar et al., 2016). MAIAC and MODIS DB presented similar statistical evaluation metrics against AERONET in the western USA during this burning period (August 2013). The MAIAC algorithm is a useful tool, especially for high-resolution studies, but in this study, it underestimated peak AOD for the most intense smoke plumes. The PIH products evaluated have great potential to improve the horizontal and vertical representation of aerosols in AQ models during wildfires. Special attention to the spatial and temporal resolution of satellite retrievals, as well as to instrument calibration, should be considered for the continuity of AQ applications from one satellite mission to future ones.

Future research directions, beyond the modeling component, should include field campaigns using ground-based lidar observations and in situ measurements (e.g., CO, absorption coefficients, aeerosol concentrations) to vertically resolve the distribution of aerosol concentrations for wildfire smoke plumes and quantify the PBLH. These measurements could then be used to evaluate the new SHBLR presented in this paper. Studies are also needed to determine how aerosol optical properties can enhance or depress PBLH from locally generated and transported smoke plumes to improve the modeled PBLH for forecasting wildfire smoke events and health effects studies.

Data Availability Statement

The MODIS, VIIRS, CALIPSO (https://earthdata.nasa.gov), AERONET (https://aeronet.gsfc.nasa.gov), and MPLNET (https://mplnet.gsfc.nasa.gov/) data used in this study are freely available from NASA. The authors are grateful to the AERONET and MPLNET PIs and site managers. Balloon sounding data are available from Atmospheric Soundings Wyoming Weather Website. Lidar data at the Rim Fire was provided by Dr. Craig B. Clements (craig.clements@sjsu.edu) from the Fire Weather Research Laboratory.

Acknowledgments
This material is based upon work supported by NASA NESSF (NASA Earth and Science Student Fellowship) program under Cooperative Agreement No. NNX16AN94H and the Nevada Space Grant Consortium-Research Infrastructure No. NNX15AI02H. We acknowledge high-performance computing support from Yellowstone (ark:/85065/d7wd3xhc) provided by NCAR's Computational and Information Systems Laboratory, sponsored by the National Science Foundation. The authors thank KC King (M.Sc.) for assistance with balloon sounding data processing, University of Nevada-Reno (UNR) graduate student Jayne M. Boehmler (M.Sc.), who downloaded albedo datasets and helped with HYSPLIT back-trajectories, and UNR undergraduate student James D. Long for help processing PBLH data from balloon soundings. Note: This work started as a collaboration between the University of Nevada, Reno, and NASA, and was completed at the University of Oklahoma.

References

Alman, B. L., Pfister, G., Hao, H., Stowell, J., Hu, X., Liu, Y., & Strickland, M. J. (2016). The association of wildfire smoke with respiratory and cardiovascular emergency department visits in Colorado in 2012: A case crossover study. *Environmental Health*, *15*(1), 64. https://doi.org/10.1186/s12940-016-0146-8

Angstrom, A. (1929). On the atmospheric transmission of sun radiation and on dust in the air. *Geografiska Annaler*, *11*, 156–166. https://doi.org/10.2307/519399

Appel, K. W., Gilliam, R. C., Davis, N., Zubrow, A., & Howard, S. C. (2011). Overview of the atmospheric model evaluation tool (AMET) v1.1 for evaluating meteorological and air quality models. *Environmental Modelling & Software*, *26*(4), 434–443. https://doi.org/10.1016/j.envsoft.2010.09.007

Baker, K. R., Woody, M. C., Valin, L., Szykman, J., Yates, E. L., Iraci, L. T., et al. (2018). Photochemical model evaluation of 2013 California wild fire air quality impacts using surface, aircraft, and satellite data. *The Science of the Total Environment*, *637–638*, 1137–1149. https://doi.org/10.1016/j.scitotenv.2018.05.048

Beck, J. A., Alexander, M. E., Harvey, S. D., & Beaver, A. K. (2002). Forecasting diurnal variations in fire intensity to enhance wildland firefighter safety. *International Journal of Wildland Fire*, *11*(4), 173–182. https://doi.org/10.1071/wf02002

Bian, Q., Ford, B., Pierce, J. R., & Kreidenweis, S. M. (2020). A decadal climatology of chemical, physical, and optical properties of ambient smoke in the western and southeastern United States. *Journal of Geophysical Research: Atmospheres*, *125*(1), e2019JD031372. https://doi.org/10.1029/2019JD031372

Blunden, J., & Arndt, D. S. (2020). State of the Climate in 2019. *Bulletin of the American Meteorological Society*, *101*(8), S1–S429. https://doi.org/10.1175/2020BAMSStateoftheClimate.1

Boehmler, J., Loría-Salazar, S., Stevens, C., Long, J., Watts, A., Holmes, H., et al. (2018). Development of a multispectral albedometer and deployment on an unmanned aircraft for evaluating satellite retrieved surface reflectance over Nevada's Black Rock Desert. *Sensors*, *18*(10, 3504. https://doi.org/10.3390/s18103504

Brewer, M. J., & Clements, C. B. (2020). The 2018 camp fire: Meteorological analysis using in situ observations and numerical simulations. *Atmosphere*, *11*(1), 47. https://doi.org/10.3390/atmos11010047

Brey, S. J., Ruminski, M., Atwood, S. A., & Fischer, E. V. (2018). Connecting smoke plumes to sources using hazard mapping system (HMS) smoke and fire location data over North America. *Atmospheric Chemistry and Physics*, *18*(3), 1745–1761. https://doi.org/10.5194/acp-18-1745-2018

Campbell, J. R., Hlavka, D. L., Welton, E. J., Flynn, C. J., Turner, D. D., Spinhirne, J. D., et al. (2002). Full-time, eye-safe cloud and aerosol lidar observation at atmospheric radiation measurement program sites: Instruments and data processing. *Journal of Atmospheric and Oceanic Technology*, *19*(4), 431–442. https://doi.org/10.1175/1520-0426(2002)019<0431:FTESCA>2.0.CO;2

Carroll, M. L., DiMiceli, C. M., Townshend, J. R. G., Sohlberg, R. A., Elders, A. I., Devadiga, S., et al. (2017). Development of an operational land water mask for MODIS Collection 6, and influence on downstream data products. *International Journal of Digital Earth*, *10*(2), 207–218. https://doi.org/10.1080/17538947.2016.1232756

Cascio, W. E. (2017). Wildland fire smoke and human health. *The Science of the Total Environment*, *624*, 586–595. https://doi.org/10.1016/j.scitotenv.2017.12.086

Chang, J. C., & Hanna, S. R. (2004). Air quality model performance evaluation. *Meteorology and Atmospheric Physics*, *87*(1–3), 167–196. https://doi.org/10.1007/s00703-003-0070-7

Cheeseman, M., Ford, B., Volckens, J., Lyapustin, A., & Pierce, J. R. (2020). The relationship between MAIAC smoke plume heights and surface PM. *Geophysical Research Letters*, *47*(17), e2020GL088949. https://doi.org/10.1029/2020GL088949

Chung, A., Chang, D. P. Y., Kleeman, M. J., Perry, K. D., Cahill, T. A., Dutcher, D., et al. (2001). Comparison of real-time instruments used to monitor airborne particulate matter. *Journal of the Air & Waste Management Association*, *51*(1), 109–120. https://doi.org/10.1080/10473289.2001.10464254

Clements, C. B., & Oliphant, A. J. (2014). The California State university mobile atmospheric profiling system: A facility for research and education in boundary layer meteorology. *Bulletin of the American Meteorological Society*, *95*(11), 1713–1724. https://doi.org/10.1175/BAMS-D-13-00179.1

Crockett, J. L., & Westerling, A. L. (2017). Greater temperature and precipitation extremes intensify western U.S. droughts, wildfire severity, and Sierra Nevada Tree mortality. *Journal of Climate*, *31*(1), 341–354. https://doi.org/10.1175/JCLI-D-17-0254.1

Draxler, R. R., & Rolph, G. D. (2013). *Air resources laboratory–HYSPLIT–hybrid single particle lagrangian integrated trajectory model*. http://ready.arl.noaa.gov/HYSPLIT.php

Eck, T. F., Holben, B. N., Reid, J. S., Dubovik, O., Smirnov, A., O'Neill, N. T., et al. (1999). Wavelength dependence of the optical depth of biomass burning, urban, and desert dust aerosols. *Journal of Geophysical Research*, *104*(D24), 31333–31349. https://doi.org/10.1029/1999JD900923

Eck, T. F., Holben, B. N., Reid, J. S., Mukelabai, M. M., Piketh, S. J., Torres, O., et al. (2013). A seasonal trend of single scattering albedo in southern African biomass-burning particles: Implications for satellite products and estimates of emissions for the world's largest biomass-burning source. *Journal of Geophysical Research: Atmospheres*, *118*(12), 6414–6432. https://doi.org/10.1002/jgrd.50500

EPA 454/R-08-003. (2008). *Air quality modeling platform for the ozone national ambient air quality standard final rule regulatory impact analysis* (pp. 1–17). Research Triangle Park: U.S. Environmental Protection Agency. http://www3.epa.gov/scram001/reports/O3%20NAAQS%20Final%20Rule%20RIA%20AQModeling%20Platform%20_03-11-08.pdf

Fisher, D., Wooster, M. J., Xu, W., Thomas, G., & Lestari, P. (2020). Top-down estimation of particulate matter emissions from extreme tropical peatland fires using geostationary satellite fire radiative power observations. *Sensors*, *20*(24), 7075. https://doi.org/10.3390/s20247075

Giglio, L. (2007). Characterization of the tropical diurnal fire cycle using VIRS and MODIS observations. *Remote Sensing of Environment*, *108*(4), 407–421. https://doi.org/10.1016/j.rse.2006.11.018

Giglio, L., Schroeder, W., & Justice, C. O. (2016). The collection 6 MODIS active fire detection algorithm and fire products. *Remote Sensing of Environment*, *178*, 31–41. https://doi.org/10.1016/j.rse.2016.02.054

Giles, D. M., Sinyuk, A., Sorokin, M. G., Schafer, J. S., Smirnov, A., Slutsker, I., et al. (2019). Advancements in the Aerosol Robotic Network (AERONET) Version 3 database - automated near-real-time quality control algorithm with improved cloud screening for Sun photometer aerosol optical depth (AOD) measurements. *Atmosphere Measure Technique*, *12*(1), 169–209. https://doi.org/10.5194/amt-12-169-2019

Griffin, R. J., Cocker, D. R., Flagan, R. C., & Seinfeld, J. H. (1999). Organic aerosol formation from the oxidation of biogenic hydrocarbons. *Journal of Geophysical Research*, *104*(D3), 3555–3567. https://doi.org/10.1029/1998JD100049

Gupta, P., Christopher, S. A., Wang, J., Gehrig, R., Lee, Y., & Kumar, N. (2006). Satellite remote sensing of particulate matter and air quality assessment over global cities. *Atmospheric Environment*, *40*(30), 5880–5892. https://doi.org/10.1016/j.atmosenv.2006.03.016

Hao, W. M., & Larkin, N. K. (2014). Wildland fire emissions, carbon, and climate: Wildland fire detection and burned area in the United States. *Forest Ecology and Management*, *317*, 20–25. https://doi.org/10.1016/j.foreco.2013.09.029

Hoffmann, T., Odum, J. R., Bowman, F., Collins, D., Klockow, D., Flagan, R. C., & Seinfeld, J. H. (1997). Formation of organic aerosols from the oxidation of biogenic hydrocarbons. *Journal of Atmospheric Chemistry*, *26*, 189, 222. https://doi.org/10.1023/A:1005734301837

Hoff, R. M., & Christopher, S. A. (2009). Remote sensing of particulate pollution from space: Have we reached the promised land?, *Journal of the Air & Waste Management Association*, *59*(6), 645–675. https://doi.org/10.3155/1047-3289.59.6.645

Holben, B. N., Eck, T. F., Slutsker, I., Tanré, D., Buis, J. P., Setzer, A., et al. (1998). AERONET-A federated instrument network and data archive for aerosol characterization. *Remote Sensing of Environment*, *66*(1), 1–16. https://doi.org/10.1016/S0034-4257(98)00031-5

Holben, B. N., Tanré, D., Smirnov, A., Eck, T. F., Slutsker, I., Abuhassan, N., et al. (2001). An emerging ground-based aerosol climatology: Aerosol optical depth from AERONET. *Journal of Geophysical Research*, *106*(D11), 12067–12097. https://doi.org/10.1029/2001JD900014

Hsu, N. C., Jeong, M.-J., Bettenhausen, C., Sayer, A. M., Hansell, R., Seftor, C. S., et al. (2013). Enhanced Deep Blue aerosol retrieval algorithm: The second generation. *Journal of Geophysical Research - D: Atmospheres*, *118*(16), 9296–9315. https://doi.org/10.1002/jgrd.50712

Hsu, N. C., Lee, J., Sayer, A. M., Kim, W., Bettenhausen, C., & Tsay, S. C. (2019). VIIRS Deep Blue aerosol products over land: Extending the EOS long-term aerosol data records. *Journal of Geophysical Research: Atmospheres*, *124*(7), 4026–4053. https://doi.org/10.1029/2018JD029688

Huang, J., Arnott, W. P., Barnard, J. C., & Holmes, H. A. (2021). Theoretical uncertainty analysis of satellite retrieved aerosol optical depth associated with surface albedo and aerosol optical properties. *Remote Sensing*, *13*(3), 344. https://doi.org/10.3390/rs13030344

Hu, X., Waller, L. A., Lyapustin, A., Wang, Y., Al-Hamdan, M. Z., Crosson, W. L., et al. (2014). Estimating ground-level $PM_{2.5}$ concentrations in the southeastern United States using MAIAC AOD retrievals and a two-stage model. *Remote Sensing of Environment*, *140*, 220–232. https://doi.org/10.1016/j.rse.2013.08.032

Jeong, M.-J., & Hsu, N. C. (2008). Retrievals of aerosol single-scattering albedo and effective aerosol layer height for biomass-burning smoke: Synergy derived from "A-Train" sensors. *Geophysical Research Letters*, *35*(24), L24801. https://doi.org/10.1029/2008GL036279

Kahn, R. A., Li, W.-H., Moroney, C., Diner, D. J., Martonchik, J. V., & Fishbein, E. (2007). Aerosol source plume physical characteristics from space-based multiangle imaging. *Journal of Geophysical Research*, *112*(D11). https://doi.org/10.1029/2006JD007647

Kaiser, J. W., Heil, A., Andreae, M. O., Benedetti, A., Chubarova, N., Jones, L., et al. (2012). Biomass burning emissions estimated with a global fire assimilation system based on observed fire radiative power. *Biogeosciences*, *9*(1), 527–554. https://doi.org/10.5194/bg-9-527-2012

Kim, M.-H., Omar, A. H., Tackett, J. L., Vaughan, M. A., Winker, D. M., Trepte, C. R., et al. (2018). The CALIPSO version 4 automated aerosol classification and lidar ratio selection algorithm. *Atmosphere Measure Technique*, *11*(11), 6107–6135. https://doi.org/10.5194/amt-11-6107-2018

Kogan, F., & Guo, W. (2015). 2006–2015 mega-drought in the western USA and its monitoring from space data. *Geomatics, Natural Hazards and Risk*, *6*(8), 651–668. https://doi.org/10.1080/19475705.2015.1079265

Lee, J., Hsu, N. C., Bettenhausen, C., Sayer, A. M., Seftor, C. J., & Jeong, M. J. (2015). Retrieving the height of smoke and dust aerosols by synergistic use of VIIRS, OMPS, and CALIOP observations. *Journal of Geophysical Research: Atmospheres*, *120*(16), 8372, 8388. https://doi.org/10.1002/2015JD023567

Lee, J., Hsu, N. C., Bettenhausen, C., Sayer, A. M., Seftor, C. J., Jeong, M. J., et al. (2016). Evaluating the height of biomass burning smoke aerosols retrieved from synergistic use of multiple satellite sensors over southeast Asia. *Aerosol and Air Quality Research*, *16*(11), 2831–2842. https://doi.org/10.4209/aaqr.2015.08.0506

Li, F., Zhang, X., Kondragunta, S., & Csiszar, I. (2018). Comparison of fire radiative power estimates from VIIRS and MODIS observations. *Journal of Geophysical Research: Atmospheres*, *123*(9), 4545–4563. https://doi.org/10.1029/2017JD027823

Li, J., Carlson, B. E., & Lacis, A. A. (2015). How well do satellite AOD observations represent the spatial and temporal variability of $PM_{2.5}$ concentration for the United States? *Atmospheric Environment*, *102*, 260–273. https://doi.org/10.1016/j.atmosenv.2014.12.010

Lim, S. S., Vos, T., Flaxman, A. D., Danaei, G., Shibuya, K., Adair-Rohani, H., et al. (2012). A comparative risk assessment of burden of disease and injury attributable to 67 risk factors and risk factor clusters in 21 regions, 1990–2010: A systematic analysis for the global burden of disease study 2010. *The Lancet*, *380*(9859), 2224–2260. https://doi.org/10.1016/S0140-6736(12)61766-8

Liu, C., Fedorovich, E., Huang, J., Hu, X.-M., Wang, Y., & Lee, X. (2019a). Impact of aerosol shortwave radiative heating on entrainment in the atmospheric convective boundary layer: A large-eddy simulation study. *Journal of the Atmospheric Sciences*, *76*(3), 785–799. https://doi.org/10.1175/JAS-D-18-0107.1

Liu, C., Huang, J., Fedorovich, E., Hu, X.-M., Wang, Y., & Lee, X. (2018). The effect of aerosol radiative heating on turbulence statistics and spectra in the atmospheric convective boundary layer: A large-eddy simulation study. *Atmosphere*, *9*(9), 347. https://doi.org/10.3390/atmos9090347

Liu, Y., Kochanski, A., Baker, K. R., Mell, W., Linn, R., Paugam, R., et al. (2019b). Fire behaviour and smoke modelling: Model improvement and measurement needs for next-generation smoke research and forecasting systems. *International Journal of Wildland Fire*, *28*(28), 570–588. https://doi.org/10.1071/WF18204

Li, Z., Guo, J., Ding, A., Liao, H., Liu, J., Sun, Y., et al. (2017). Aerosol and boundary-layer interactions and impact on air quality. *National Science Review*, *4*(6), 810–833. https://doi.org/10.1093/nsr/nwx117

Loría-Salazar, S. M., Holmes, H. A., Patrick Arnott, W., Barnard, J. C., & Moosmüller, H. (2016). Evaluation of MODIS columnar aerosol retrievals using AERONET in semi-arid Nevada and California, U.S.A., during the summer of 2012. *Atmospheric Environment*, *144*, 345–360. https://doi.org/10.1016/j.atmosenv.2016.08.070

Loría-Salazar, S. M., Panorska, A., Arnott, W. P., Barnard, J. C., Boehmler, J. M., & Holmes, H. A. (2017). Toward understanding atmospheric physics impacting the relationship between columnar aerosol optical depth and near-surface PM mass concentrations in Nevada and California, U.S.A., during 2013. *Atmospheric Environment*, *171*, 289–300. https://doi.org/10.1016/j.atmosenv.2017.10.023

Lyapustin, A. I., Wang, Y., Laszlo, I., Hilker, T., Hall, G. F., Sellers, P. J., et al. (2012). Multi-angle implementation of atmospheric correction for MODIS (MAIAC): 3. Atmospheric correction. *Remote Sensing of Environment*, *127*, 385–393. https://doi.org/10.1016/j.rse.2012.09.002

Lyapustin, A., Wang, Y., Korkin, S., & Huang, D. (2018). MODIS Collection 6 MAIAC algorithm. *Atmosphere Measure Techniques*, *11*(10), 5741–5765. https://doi.org/10.5194/amt-11-5741-2018

Lyapustin, A., Wang, Y., Korkin, S., Kahn, R., & Winker, D. (2020). MAIAC thermal technique for smoke injection height from MODIS. *IEEE Geoscience and Remote Sensing Letters*, *17*(5), 730–734. https://doi.org/10.1109/LGRS.2019.2936332

Michalakes, J., Dudhia, D., Gill, D., Klemp, J., & Skamarock, W. (1998). *Design of a next-generation regional weather research and forecast model*. United States.

Michalakes, J. J., Dudhia, D., Gill, T., Henderson, J., Klemp, W., Skamarock, W., & Wang, W. (2004). The weather research and forecast model: Software architecture and performance. In *Presented at the Proceedings of the 11th ECMWF Workshop on the Use of high performance computing in meteorology*. George Mozdzynski.

Murray, N. L., Holmes, H. A., Liu, Y., & Chang, H. H. (2019). A Bayesian ensemble approach to combine $PM_{2.5}$ estimates from statistical models using satellite imagery and numerical model simulation. *Environmental Research*, *178*, 108601. https://doi.org/10.1016/j.envres.2019.108601

Nabavi, S. O., Haimberger, L., & Abbasi, E. (2019). Assessing $PM_{2.5}$ concentrations in Tehran, Iran, from space using MAIAC, deep blue, and dark target AOD and machine learning algorithms. *Atmospheric Pollution Research*, *10*(3), 889–903. https://doi.org/10.1016/j.apr.2018.12.017

Parrish, D. D., Aikin, K. C., Oltmans, S. J., Johnson, B. J., Ives, M., & Sweeny, C. (2010). Impact of transported background ozone inflow on summertime air quality in a California ozone exceedance area. *Atmospheric Chemistry and Physics*, *10*(20), 10093–10109. https://doi.org/10.5194/acp-10-10093-2010

Paugam, R., Wooster, M., Freitas, S., & Val Martin, M. (2016). A review of approaches to estimate wildfire plume injection height within large-scale atmospheric chemical transport models. *Atmospheric Chemistry and Physics*, *16*(2), 907–925. https://doi.org/10.5194/acp-16-907-2016

Peterson, D. A., Fromm, M. D., Solbrig, J. E., Hyer, E. J., Surratt, M. L., &, Campbell, J. R. (2017). Detection and inventory of intense pyroconvection in western North America using GOES-15 daytime infrared data. *Journal of Applied Meteorology and Climatology*, *56*(2), 471–493. https://doi.org/10.1175/JAMC-D-16-0226.1

Peterson, D. A., Hyer, E. J., Campbell, J. R., Fromm, M. D., Hair, J. W., Butler, C. F., & Fenn, M. A. (2014). The 2013 rim fire: Implications for predicting extreme fire spread, pyroconvection, and smoke emissions. *Bulletin of the American Meteorological Society*, *96*(2), 229–247. https://doi.org/10.1175/BAMS-D-14-00060.1

Pierce, A. M., Gustin, M. S., Christensen, J. N., & Loría-Salazar, S. M. (2018). Use of multiple tools including lead isotopes to decipher sources of ozone and reactive mercury to urban and rural locations in Nevada, USA. *The Science of the Total Environment*, *615*, 1411–1427. https://doi.org/10.1016/j.scitotenv.2017.08.284

Pierce, A. M., Loría-Salazar, S. M., Holmes, H. A., & Gustin, M. S. (2019) Investigating horizontal and vertical pollution gradients in the atmosphere associated with an urban location in complex terrain, Reno, Nevada, USA. *Atmospheric Environment*. *196*, 103–117. https://doi.org/10.1016/j.atmosenv.2018.09.063

Pitchford, M., Malm, W., Schichtel, B., Kumar, N., Lowenthal, D., & Hand, J. (2007). Revised algorithm for estimating light extinction from IMPROVE particle speciation data. *Journal of the Air & Waste Management Association*, *57*(11), 1326–1336. https://doi.org/10.3155/1047-3289.57.11.1326

Saide, P. E., Peterson, D. A., da Silva, A., Anderson, B., Ziemba, L. D., Diskin, G., et al. (2015). Revealing important nocturnal and day-to-day variations in fire smoke emissions through a multiplatform inversion. *Geophysical Research Letters*, *42*(9), 3609–3618. https://doi.org/10.1002/2015GL063737

Sayer, A. M. (2020). How long is too long? Variogram analysis of AERONET data to aid aerosol validation and intercomparison studies. *Earth and Space Science*, *7*(9), e2020EA001290. https://doi.org/10.1029/2020EA001290

Sayer, A. M., Hsu, N. C., Bettenhausen, C., & Jeong, M.-J. (2013). Validation and uncertainty estimates for MODIS Collection 6 "Deep Blue" aerosol data. *Journal of Geophysical Research: Atmospheres*, *118*(14), 7864–7872. https://doi.org/10.1002/jgrd.50600

Sayer, A. M., Hsu, N. C., Eck, T. F., Smirnov, A., & Holben, B. N. (2014). AERONET-based models of smoke-dominated aerosol near source regions and transported over oceans, and implications for satellite retrievals of aerosol optical depth. *Atmospheric Chemistry and Physics*, *14*(20), 11493–11523. https://doi.org/10.5194/acp-14-11493-2014

Sayer, A. M., Hsu, N. C., Lee, J., Kim, W. V., & Dutcher, S. T. (2019). Validation, stability, and consistency of MODIS Collection 6.1 and VIIRS Version 1 Deep Blue aerosol data over land. *Journal of Geophysical Research: Atmospheres*, *124*, 4658, 4688. https://doi.org/10.1029/2018JD029598

Scasta, J. D., Weir, J. R., & Stambaugh, M. C. (2016). Droughts and wildfires in western U.S. Rangelands. *Rangelands*, *38*(4), 197–203. https://doi.org/10.1016/j.rala.2016.06.003

Schaaf, C. B., Gao, F., Strahler, A. H., Lucht, W., Li, X., Tsang, T., et al. (2002). First operational BRDF, albedo nadir reflectance products from MODIS. *Remote Sensing of Environment*, *83*(1–2), 135–148. https://doi.org/10.1016/S0034-4257(02)00091-3

Shi, Y. R., Levy, R. C., Eck, T. F., Fisher, B., Mattoo, S., Remer, L. A., et al. (2019). Characterizing the 2015 Indonesia fire event using modified MODIS aerosol retrievals. *Atmospheric Chemistry and Physics*, *19*(1), 259–274. https://doi.org/10.5194/acp-19-259-2019

Simon, H., Baker, K. R., & Phillips, S. (2012). Compilation and interpretation of photochemical model performance statistics published between 2006 and 2012. *Atmospheric Environment*, *61*, 124–139. https://doi.org/10.1016/j.atmosenv.2012.07.012

Snider, G., Weagle, C. L., Martin, R. V., van Donkelaar, A., Conrad, K., Cunningham, D., et al. (2015). SPARTAN: A global network to evaluate and enhance satellite-based estimates of ground-level particulate matter for global health applications. *Atmospheric Measurements Techniques*, *8*(1), 505–521. https://doi.org/10.5194/amt-8-505-2015

Sofiev, M., Vankevich, R., Lotjonen, M., Prank, M., Petukhov, V., Ermakova, T., et al. (2009). An operational system for the assimilation of the satellite information on wild-land fires for the needs of air quality modelling and forecasting. *Atmospheric Chemistry and Physics*, *9*(18), 6833–6847. https://doi.org/10.5194/acp-9-6833-2009

Stephens, S. L., & Collins, B. M. (2004). Fire regimes of mixed conifer forests in the north-central Sierra Nevada at multiple spatial scales. *Northwest Science*, *78*, 12–23.

Stephens, S. L., & Fry, D. L. (2005). Fire history in coast redwood stands in the northeastern Santa Cruz Mountains, California. *Fire Ecology*, *1*(1), 2–19. https://doi.org/10.4996/fireecology.0101002

Stocker, T. F., Qin, D., Plattner, G.-K., Tignor, M., Allen, S. K., Boschung, J., et al. (2013). IPCC, 2013: Climate Change 2013: The Physical Science Basis. Contribution of Working Group I to the Fifth Assessment Report of the Intergovernmental Panel on Climate Change. Cambridge: Cambridge University Press. https://doi.org/10.1017/CBO9781107415324

Streets, D. G., Canty, T., Carmichael, G. R., de Foy, B., Dickerson, R. R., Duncan, B. N., et al. (2013). Emissions estimation from satellite retrievals: A review of current capability. *Atmospheric Environment*, *77*, 1011–1042. https://doi.org/10.1016/j.atmosenv.2013.05.051

Stull, R. B. (1988). *An introduction to boundary layer meteorology*. Springer Science & Business Media.

US Drought Monitor (2020). *Drought.gov*. https://www.drought.gov/drought/data-gallery/us-drought-monitor

Wang, J., & Christopher, S. A. (2003). Intercomparison between satellite-derived aerosol optical thickness and $PM_{2.5}$ mass: Implications for air quality studies. *Geophysical Research Letters*, *30*(21), 2095. https://doi.org/10.1029/2003GL018174

Welton, E. J., Campbell, J. R., Spinhirne, J. D., & Scott, III. V. S. (2001). *Global monitoring of clouds and aerosols using a network of micropulse lidar systems*. Presented at The Society of Photo-Optical Instrumentation Engineers (SPIE) Conference Series (Vol. 4153, pp. 151–158).

Westerling, A. L. (2016). Increasing western US forest wildfire activity: Sensitivity to changes in the timing of spring. *Philosophical Transactions of the Royal Society B: Biological Sciences*, *371*, 20150178. https://doi.org/10.1098/rstb.2015.0178

Westerling, A. L., Hidalgo, H. G., Cayan, D. R., & Swetnam, T. W. (2006). Warming and earlier spring increase western U.S. forest wildfire activity. *Science*, *313*(5789), 940–943. https://doi.org/10.1126/science.1128834

Wilkins, J. L., Foy, B. D., Thompson, A. M., Peterson, D. A., Hyer, E. J., Graves, C., et al. (2020). Evaluation of stratospheric intrusions and biomass burning plumes on the vertical distribution of tropospheric ozone over the midwestern United States. *Journal of Geophysical Research: Atmospheres*, *125*(18), e2020JD032454. https://doi.org/10.1029/2020JD032454

Wilkins, J. L., Pouliot, G., Foley, K., Appel, W., & Pierce, T. (2018). The impact of US wildland fires on ozone and particulate matter: a comparison of measurements and CMAQ model predictions from 2008 to 2012. *International Journal of Wildland Fire*, *27*(10), 684–698. https://doi.org/10.1071/WF18053

Winker, D. M., Pelon, J., Coakley, J. A., Ackerman, S. A., Charlson, R. J., Colarco, P. R., et al. (2010). The CALIPSO mission: A global 3D view of aerosols and clouds. *Bulletin of the American Meteorological Society*, *91*(9), 1211–1229. https://doi.org/10.1175/2010BAMS3009.1

Yates, E. L., Iraci, L. T., Singh, H. B., Tanaka, T., Roby, M. C., Hamill, P., et al. (2016). Airborne measurements and emission estimates of greenhouse gases and other trace constituents from the 2013 California Yosemite Rim wildfire. *Atmospheric Environment*, *127*, 293–302. https://doi.org/10.1016/j.atmosenv.2015.12.038

Zoogman, P., Liu, X., Suleiman, R. M., Pennington, W. F., Flittner, D. E., Al-Saadi, J. A., et al. (2017). Tropospheric emissions: Monitoring of pollution (TEMPO). *Journal of Quantitative Spectroscopy and Radiative Transfer*, *186*, 17–39. https://doi.org/10.1016/j.jqsrt.2016.05.008